



CERN-EP-2018-201
16 July 2018

Medium modification of the shape of small-radius jets in central Pb–Pb collisions at $\sqrt{s_{\text{NN}}} = 2.76$ TeV

ALICE Collaboration*

Abstract

We present the measurement of a new set of jet shape observables for track-based jets in central Pb–Pb collisions at $\sqrt{s_{\text{NN}}} = 2.76$ TeV. The set of jet shapes includes the first radial moment or angularity, g ; the momentum dispersion, $p_{\text{T}}D$; and the difference between the leading and sub-leading constituent track transverse momentum, $LeSub$. These observables provide complementary information on the jet fragmentation and can constrain different aspects of the theoretical description of jet-medium interactions. The jet shapes were measured for a small resolution parameter $R = 0.2$ and were fully corrected to particle level. The observed jet shape modifications indicate that in-medium fragmentation is harder and more collimated than vacuum fragmentation as obtained by PYTHIA calculations, which were validated with the measurements of the jet shapes in proton-proton collisions at $\sqrt{s} = 7$ TeV. The comparison of the measured distributions to templates for quark and gluon-initiated jets indicates that in-medium fragmentation resembles that of quark jets in vacuum. We further argue that the observed modifications are not consistent with a totally coherent energy loss picture where the jet loses energy as a single colour charge, suggesting that the medium resolves the jet structure at the angular scales probed by our measurements ($R = 0.2$). Furthermore, we observe that small- R jets can help to isolate purely energy loss effects from other effects that contribute to the modifications of the jet shower in medium such as the correlated background or medium response.

© 2018 CERN for the benefit of the ALICE Collaboration.

Reproduction of this article or parts of it is allowed as specified in the CC-BY-4.0 license.

*See Appendix A for the list of collaboration members

1 Introduction

The objective of the heavy-ion jet physics program at RHIC and LHC is to understand the behaviour of QCD matter at the limit of high energy density and temperature by studying the dynamics of jet-medium interactions. Jet physics in heavy-ion collisions is a multiscale problem. Hard scales govern the elementary scattering and the subsequent branching process down to non-perturbative scales, in the vacuum as well as in the medium. Soft scales, of the order of the temperature of the medium, characterise the interactions of soft partons produced in the shower with the strongly coupled medium. Soft scales also rule hadronisation, which is expected to take place in vacuum for sufficiently energetic probes. A detailed discussion of the different processes contributing to the jet shower evolution in medium and their onset scales can be found in Ref. [1]. The interplay between these processes can lead to modifications of the longitudinal and transverse distributions of the constituents of the jet with respect to jet fragmentation in vacuum. These jet structure modifications can be investigated with jet shape observables and have the potential to constrain the dynamics of jet energy loss in medium, the role of colour coherence [2], and fundamental medium properties like temperature, density or the evolution of the medium degrees of freedom with the resolution scale [3].

The jet shape observables measured so far in heavy-ion collisions at the LHC can be classified into three groups: inclusive, jet-by-jet shapes using constituents information, and jet shapes using the clustering history. The first group consists on inclusive observables that measure intra or inter-jet distributions. The ratios of jet yields with different resolution parameter R are an example. Such ratios are infrared and collinear (IRC) safe [4] and are sensitive to the transverse energy profile of the jets [5–7]. ATLAS measured central to peripheral inclusive jet yield ratios for different jet radii up to $R = 0.5$ showing differences of the order of 30% at $p_{T,\text{jet}} < 100$ GeV/ c [8], which indicate energy redistribution within the jet in medium relative to vacuum. In ALICE, such ratios were measured for inclusive and semi-inclusive samples of jets recoiling from high- p_T hadrons [9, 10]. In the case of recoil jets, larger R were accessible and the results showed no indication of medium modifications when changing the jet resolution up to $R = 0.5$. ALICE and ATLAS measurements are characterised by different jet selections and different minimum constituent cutoffs. Another example of shapes belonging to this category are the fragmentation functions [11, 12]. The fragmentation functions give information on the longitudinal share of energy within the jet. The experimental results show an enhancement of the low and high- z component and a depletion at intermediate z in Pb–Pb relative to pp collisions, where z is the fraction of the jet momentum carried by the particles in the jet [11, 12]. The modifications are small and they were quantified as an excess of approximately 0.9 particles at low momentum, in the difference between the integrals of the fragmentation functions in Pb–Pb and pp collisions.

In order to probe the jet shape at large angles relative to the jet axis, two observables were designed. The CMS missing p_T method [13] considers the projection of all particle momentum vectors in the event onto the axis of a selected dijet pair. This method is insensitive to the uncorrelated background, and particles correlated with the dijet reveal that momentum balance of the system is totally recovered only by very soft particles ($p_T \leq 1$ GeV/ c) at large angles ($\Delta R_{\text{jet}} > 0.8$). Jet-track angular correlations [14] explore the large-angle component differentially with similar conclusions. Similarly, the jet profile [15] measures the radial distribution of energy relative to the jet axis. The results indicate an enhancement of momentum relative to pp collisions at distances to the jet axis $\Delta R_{\text{jet}} \gtrsim 0.3$. This enhancement is accompanied by a reduction of momentum at short distances to the jet axis $0.1 < \Delta R_{\text{jet}} < 0.2$.

The second group of shape observables are the jet shapes built as a jet-by-jet function of the jet constituent 4-momenta. The jet mass [16] is an example. The jet mass is related to the virtuality of the parton that originated the jet. It increases with large-angle soft particle emission. The ALICE measurement of the jet mass in heavy-ion collisions [16] for jets of $R = 0.4$ showed a hint of reduction relative to the vacuum reference. Theoretical models show that energy loss effects reduce the jet mass while the medium response increases it, resulting in a mass that is shifted to higher values than what was found by

ALICE results [17].

The third category of jet shape observables uses the clustering history to select certain parts of the particle shower using well-defined jet clustering techniques, for instance grooming [18, 19], to amplify or suppress a region of the splitting phase space where medium-induced effects are expected. Examples are the 2-subjetiness [20] or the soft drop subjet momentum balance, z_g [21, 22], designed to explore changes in the rate of 2-prong jets and the momentum balance of semi-hard subjets in heavy-ion collisions relative to pp collisions. New ideas and applications for this third category of jet shapes are being discussed in the literature for beyond Standard Model searches and QCD studies in pp as well as heavy-ion collisions.

The shapes analysed in this paper belong to the second category and are described in detail in Section 2. They probe complementary aspects of the jet fragmentation such as the transverse energy profile or the dispersion of the jet constituents transverse momentum distribution. Our aim was to perform a systematic exploration of the intrajet distributions to pose constraints on key aspects of the theory of jet quenching. A clean connection to the theory was pursued via the selection of observables that are well defined and calculable from first principles in pQCD and via the full correction of the observables to particle level. The considered small resolution $R = 0.2$ and ALICE instrumental capabilities allowed us to obtain fully corrected particle-level jet measurements, in a unique range at the LHC of low jet momentum and low constituent momentum cutoff of 0.15 GeV/ c . Our measurements give insight on whether the jet substructure is resolved by the medium at small angular scales and on the role of the medium response.

The rest of the paper is organized as follows: Section 3 presents the data sets and event selection used for the analysis, Sections 4 and 5 describe the jet finding procedure and the underlying event subtraction, while Sections 6 and 7 present the response of the shapes to detector effects and background fluctuations and the 2-dimensional unfolding procedure that simultaneously corrects the shape and jet p_T distributions. Section 8 describes the different contributions to the systematic uncertainty and finally, Section 9 presents the fully corrected results and their interpretation with comparisons to theoretical models.

2 The set of jet shape observables

In this analysis, we focus on three jet shape observables that probe complementary aspects of the jet fragmentation, namely the first radial moment or angularity (or girth), g , the momentum dispersion, $p_T D$, and the difference between the leading and sub-leading track transverse momentum, $LeSub$.

The angularity is defined as

$$g = \sum_{i \in \text{jet}} \frac{p_{T,i}}{p_{T,\text{jet}}} \Delta R_{\text{jet},i}, \quad (1)$$

where $p_{T,i}$ is the transverse momentum of the i -th constituent and $\Delta R_{\text{jet},i}$ is the distance in (η, φ) space between constituent i and the jet axis. This shape is sensitive to the radial energy profile of the jet.

The momentum dispersion $p_T D$ is defined as

$$p_T D = \frac{\sqrt{\sum_{i \in \text{jet}} p_{T,i}^2}}{\sum_{i \in \text{jet}} p_{T,i}}. \quad (2)$$

This shape measures the second moment of the constituent p_T distribution in the jet and is connected to how hard or soft the jet fragmentation is. For example, in the extreme case of few constituents carrying a large fraction of the jet momentum, $p_T D$ will be close to 1, while in the case of jets with a large number of constituents and softer momentum, $p_T D$ would end up closer to 0.

The two previous shapes are related to the moments of the so-called generalized angularities defined as: $\lambda_\beta^\kappa = \sum_i \left(\frac{p_{T,i}}{p_{T,\text{jet}}} \right)^\kappa \left(\frac{\Delta R_{\text{jet},i}}{R} \right)^\beta$ [23]. The number of jet constituents corresponds to $(\kappa, \beta) = (0, 0)$, the square

of $p_T D$ corresponds to (2,0), the angularity g corresponds to (1,1), and the square of the mass scaled by the jet p_T is related to (1,2).

$LeSub$ is defined as the difference of the leading track p_T ($p_{T,track}^{lead}$) and sub-leading track p_T ($p_{T,track}^{sublead}$):

$$LeSub = p_{T,track}^{lead} - p_{T,track}^{sublead} \quad (3)$$

$LeSub$ is not an IRC-safe observable but shows robustness against contributions of soft background particles as we will discuss in Section 5. In order to give an illustrative example for the sensitivity of these observables to different types of jet fragmentation, Fig. 1 compares the behaviour of the shapes distributions for quark and gluon initiated jets as obtained by PYTHIA [24] in pp collisions. At the same transverse momentum, gluon jets are broader and produce more fragments with a softer momentum spectrum than quark jets. Consequently, their first radial moment (g) is on average higher, whereas the momentum dispersion ($p_T D$) and $LeSub$ are lower. The momentum dependence of the three shapes in vacuum is illustrated in Fig. 2. As the jet momentum increases, the angularity and the $p_T D$ decrease while $LeSub$ shifts to higher values. These changes are consistent with jets becoming narrower and with larger differences among constituents' transverse momentum at higher jet p_T .

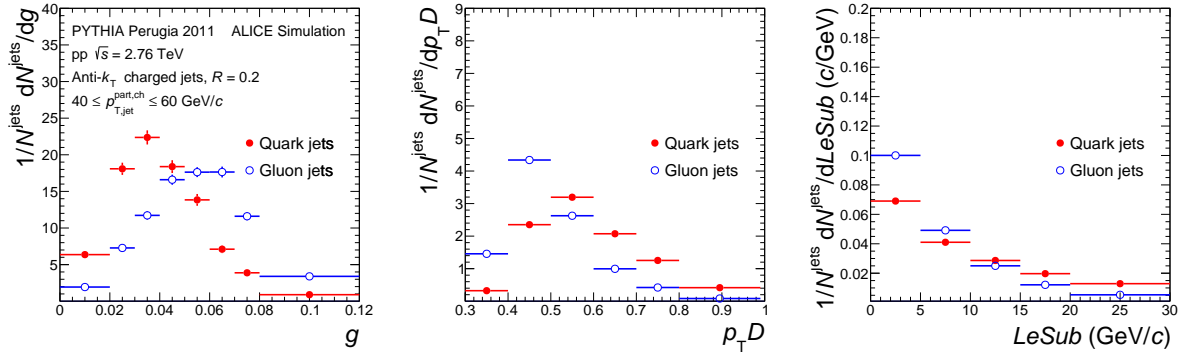


Fig. 1: g , $p_T D$, and $LeSub$ for quark and gluon jets as obtained from PYTHIA Perugia 2011 simulations of pp collisions at $\sqrt{s} = 2.76$ TeV in the transverse momentum interval $40 \leq p_{T,jet}^{part, ch} \leq 60$ GeV/c.

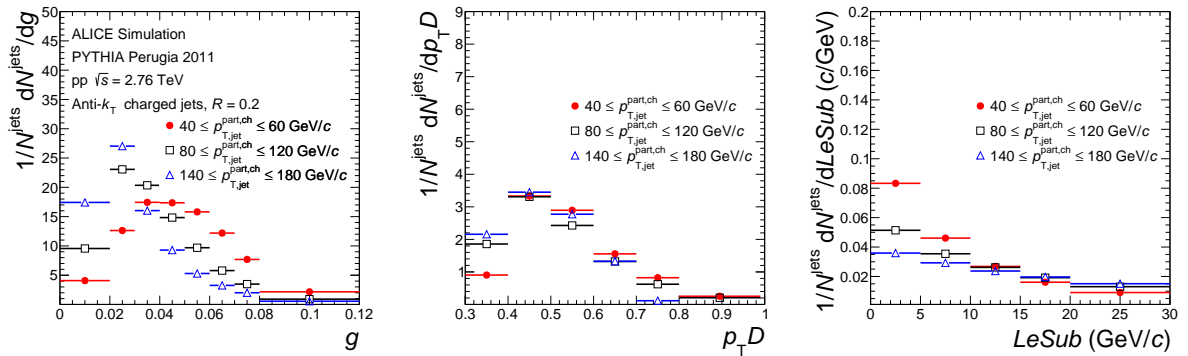


Fig. 2: g , $p_T D$, and $LeSub$ as obtained from PYTHIA Perugia 2011 simulations of pp collisions at $\sqrt{s} = 2.76$ TeV for three different transverse momentum intervals.

3 Data sets, event selection, and simulations

The ALICE detector and its performance are described in Refs. [25, 26].

The data were taken during the 2011 LHC Pb–Pb run at $\sqrt{s_{NN}} = 2.76$ TeV. This analysis uses events recorded with minimum-bias (MB) triggers, based on the signal measured in the V0 scintillators detectors that cover the full azimuth in the pseudo-rapidity intervals $-3.7 < \eta < -1.7$ and $2.8 < \eta < 5.1$. The online information of the V0 detector was also used to enhance the fraction of the 10% most-central Pb–Pb collisions. The online centrality selection has an efficiency of 100% for the 0–7% interval in centrality percentile and drops to about 80% efficiency for the 7–10% interval.

Events are reconstructed offline as described in Ref. [27]. Charged tracks are measured in the ALICE central barrel via the Inner Tracking System (ITS), which consists of six cylindrical layers of silicon detectors, and the Time Projection Chamber (TPC) with acceptance $|\eta| < 0.9$ over the full azimuth. Accepted tracks were required to have $0.15 < p_T < 100$ GeV/ c , with at least 70 space-points and at least 80% of the geometrically findable space-points in the TPC. To account for the azimuthally non-uniform response of the ITS, in this dataset, two exclusive classes of tracks were used [26]: tracks with Silicon Pixel Detector (SPD) hits (70% of all tracks in central Pb–Pb collisions and 95% in pp collisions) and, when the SPD information is not present, TPC tracks with at least one hit in the ITS, with their trajectory refitted to the primary vertex to improve the momentum resolution. The primary vertex was required to lie within 10 cm of the nominal center of the detector along the beam axis and within 1 cm of it in the transverse plane. After offline event selection, the Pb–Pb dataset consisted of 17M events in the 0–10% centrality percentile interval ($L_{\text{int}} \approx 21.3 \mu\text{b}^{-1}$).

The pp collision data used to validate PYTHIA [24] were recorded during the 2010 low-luminosity pp run at $\sqrt{s} = 7$ TeV with a MB trigger selection. The trigger configuration, offline event selection and tracking are described in Ref. [28]. After the event selection, the pp dataset consisted of 168M events ($L_{\text{int}} \approx 2.5 \text{nb}^{-1}$).

For central Pb–Pb collisions, the tracking efficiency is about 80% for $p_T > 1$ GeV/ c , decreasing to $\approx 56\%$ at $p_T = 0.15$ GeV/ c . The track momentum resolution is around 1% at $p_T = 1$ GeV/ c and $\approx 2.5\%$ at $p_T = 40$ GeV/ c . For pp collisions, the tracking efficiency is about 2–3% higher than in central Pb–Pb collisions. The track momentum resolution is about 1% for reconstructed tracks with $p_T = 1$ GeV/ c and of the order of 4.1% for $p_T = 40$ GeV/ c [26, 28].

Simulations of pp collisions were carried out using PYTHIA 6.425 and PYTHIA 8, with the Perugia 2011 and 4C tunes [29]. They were used as particle-level references to our fully corrected jet shapes. Moreover, instrumental effects were simulated using PYTHIA Perugia 0 for the primary collision followed by a detailed particle transport and detector response simulation using GEANT3 [30]. Simulated events, which include primary particles and the daughters of strong and electromagnetic decays but not secondaries from interactions in the detector material or the daughters of weak decays from strange hadrons, are denoted as “particle level”. Simulated events, which also include instrumental effects and weak decay daughters, where reconstructed tracks are selected using the experimental cuts, are denoted as “detector level”.

4 Jet reconstruction

Jet reconstruction for both the pp and Pb–Pb analysis was carried out using the k_T and anti- k_T [31] algorithms applied to all accepted tracks. The E -scheme for recombination was used [32] and the mass of the charged pion was assumed for each track.

The jet area, A_{jet} , was calculated by the FastJet algorithm [32] using ghost particles (nearly zero- p_T particles that participate in the clustering procedure but do not modify the jet momentum) with area $A_g = 0.005$ [33]. A cut on the jet area was applied to suppress combinatorial jets while preserving high efficiency for true hard jets [34, 35]. Jet candidates were rejected if $A_{\text{jet}} < 0.07$ for $R = 0.2$. Jet candidates were accepted if fully contained in the acceptance, meaning that their centroids laid within $|\eta_{\text{jet}}| < 0.7$,

where η_{jet} is the pseudo-rapidity of the jet axis.

In pp collisions and for the considered $R = 0.2$, the change of the jet momentum due to the underlying event background is negligible. For the Pb–Pb analysis, corrections of jet p_{T} and jet shapes are needed due to the presence of large background from the underlying event. For that purpose, the jet reconstruction was carried out twice for each event. The first pass applies the k_{T} algorithm with $R = 0.2$ to estimate the density of jet-like transverse-momentum and mass due to the background, ρ and ρ_{m} , respectively, defined as:

$$\rho = \text{median} \left(\frac{p_{\text{T,jet}}^{\text{raw},i}}{A_{\text{jet}}^i} \right), \quad \rho_{\text{m}} = \text{median} \left(\frac{m_i}{A_{\text{jet}}^i} \right) \quad (4)$$

where the index i runs over all jet candidates in an event and $p_{\text{T,jet}}^{\text{raw},i}$, m_i , and A_{jet}^i are the transverse momentum, mass, and area of the i^{th} reconstructed jet. The two jets with highest $p_{\text{T,jet}}^{\text{raw},i}$ were excluded from the calculation of the median to suppress the impact of signal jets on the underlying event background estimate. The second pass, which generates jet candidates for the reported distributions, applied the anti- k_{T} algorithm with resolution parameter $R = 0.2$.

5 Average background subtraction and fake jet suppression

In order to correct the candidate jet p_{T} and shape distributions simultaneously for the average underlying event background, two different techniques were applied.

- Area-derivatives method [36]. This method is valid for any infrared and collinear safe jet reconstruction algorithm and jet shape. The event is characterised by ρ and ρ_{m} . Ghost particles are added uniformly in the acceptance, each of them mimicking a pileup-like component in a region of area A_{g} . The sensitivity of the shape to background is determined by calculating its derivatives with respect to the transverse momentum and mass of the ghosts. Given ρ , ρ_{m} , and the information on the derivatives, the value of the jet shape is then extrapolated by a Taylor series to zero background.
- Constituent subtraction method [37]. In this method, the subtraction operates particle-by-particle. Ghost particles are added uniformly to the acceptance, with finite p_{T} and mass given by: $p_{\text{T,g}} = A_{\text{g}}\rho$ and $m_{\text{g}} = A_{\text{g}}\rho_{\text{m}}$. The distance between each real jet constituent and each ghost is then computed and an iterative procedure starts, which consists of finding the closest pair. If the transverse momentum of particle i is larger than that of the ghost, the ghost is discarded and its transverse momentum is subtracted from that of the real particle. In case the transverse momentum of the ghost is larger than that of particle i , the real particle is discarded and the transverse momentum of the real particle is subtracted from the ghost transverse momentum. The same procedure applies to the mass. The procedure terminates when all jet constituents are analysed.

We note that in the case of $\rho_{\text{m}} = 0$, the jet p_{T} correction obtained with these methods coincides exactly with the standard area-based subtraction approach where $p_{\text{T,jet}}^{\text{sub}} = p_{\text{T,jet}} - \rho \times A_{\text{jet}}$. The ρ_{m} term was introduced to take into account that low- p_{T} particles from the underlying event have masses that are not negligible compared to their momenta. This component has impact on the observables related to differences between jet energy and 3-momentum like the jet mass [36] but negligible impact on the jet momentum.

The jet-by-jet constituent subtraction technique [37] was used as the primary method and the area-derivatives method was used as a systematic variation. To study the performance of the subtraction

methods, PYTHIA events at detector level were embedded into Pb–Pb events. Embedding means superimposing the PYTHIA and Pb–Pb events at track level. Figure 3 shows the shape distribution for embedded unsubtracted jets (squares), the average background-subtracted jet shapes (open circles and crosses for the two methods), and the PYTHIA detector-level distributions (full circles). The average background-subtracted embedded distributions get closer to the PYTHIA detector-level distributions than without background subtraction. The comparison was performed in the interval of reconstructed and subtracted embedded momentum, $p_{T,\text{jet}}^{\text{rec, ch}}$, of 40–60 GeV/c. Figure 3 reveals that *LeSub* is rather insensitive to modifications induced by the background. Residual differences, due to background fluctuations, were corrected using an unfolding procedure (see Section 7).

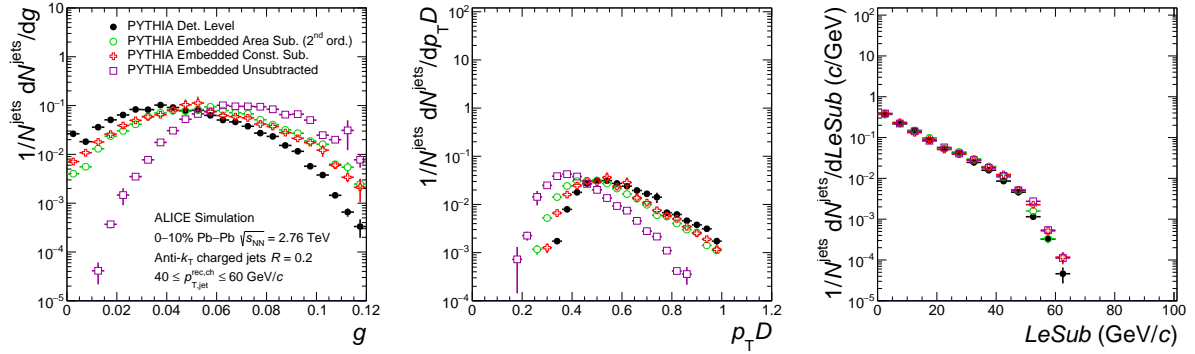


Fig. 3: Background subtraction performance for jet shapes studied with jets from PYTHIA events embedded into real Pb–Pb events, in the background subtracted transverse momentum interval $40 \leq p_{T,\text{jet}}^{\text{rec, ch}} \leq 60$ GeV/c for the area derivatives and constituent subtraction methods.

The smearing of jet p_T due to the local background fluctuations, quantified as δp_T [38], has a width of $\sigma = 4$ GeV/c for $R = 0.2$ in central Pb–Pb collisions [38]. The truncation of the raw yield at 30 GeV/c prior to unfolding sets our working point more than 7σ away from zero and thus contributions from purely combinatorial background jets to the raw spectrum are negligible, allowing for a stable unfolding correction [9].

6 Detector and background response

A 4-dimensional response matrix was built with axes $shape^{\text{part, ch}}$, $p_{T,\text{jet}}^{\text{part, ch}}$, $shape^{\text{rec, ch}}$, and $p_{T,\text{jet}}^{\text{rec, ch}}$. The upper index ‘part’ refers to particle level and ‘rec’ refers to reconstructed level quantities. In pp collisions, index ‘rec’ refers to detector-level quantities, while in Pb–Pb collisions it refers to embedded and background subtracted quantities. In order to associate a reconstructed-level jet to a particle-level jet, a matching criterion needs to be defined.

The response matrix for pp collisions is purely instrumental and was constructed using PYTHIA events at particle level and after full detector simulation. The matching criterion between the corresponding jets at particle and detector level is purely geometrical and was based on requiring that they are univocally the closest in the (η, φ) space. The response matrix for the Pb–Pb case considers both the effects of the detector and the effects of the background fluctuations. To construct it, we embedded PYTHIA detector-level events into Pb–Pb events and we applied two successive matchings, the first between the background-subtracted, embedded jets and detector-level PYTHIA jets and the second between the detector and particle-level jets. The matching between embedded and detector-level jets is not purely geometrical but also required that more than 50% of the detector-level jet momentum is contained in the embedded reconstructed jet. The matching efficiency is consistent with unity for jets with p_T above 30 GeV/c. We note that since our embedding is a superposition of PYTHIA and Pb–Pb events at track level, two-track

effects are not present, however their impact in data is small due to the large required number of clusters per track. The jet energy scale shift in pp collisions is about 15% at $p_{T,\text{jet}}^{\text{part, ch}} = 50 \text{ GeV}/c$. In Pb–Pb collisions, this shift is about 12% in the same transverse momentum range at the particle level [9]. The instrumental jet energy resolution (JER), which characterises the detector response relative to charged jets at particle level, varies from 20% at $p_{T,\text{jet}}^{\text{rec, ch}} = 20 \text{ GeV}/c$ to 25% at $p_{T,\text{jet}}^{\text{rec, ch}} = 100 \text{ GeV}/c$, similarly for pp and Pb–Pb collisions. The JER is dominated by tracking effects and shows no dependence with jet R [9].

The jet shape resolution can be studied via the distribution of residuals, which gives the relative difference between the jet shapes measured at particle and reconstructed level. In Fig. 4, the left panels show the distribution of residuals for each of the three shapes for jets in pp and for PYTHIA embedded jets in Pb–Pb collisions, in the particle-level jet $p_{T,\text{jet}}^{\text{part, ch}}$ range of 40–60 GeV/ c . Tracking inefficiency induces a negative tail in the angularity (narrower jets due to missing constituents), while a positive tail is induced on average by background fluctuations and, to a lower extent, also by track momentum resolution. The trend is the opposite in the case of $p_T D$: losses due to tracking efficiency shift the distribution of residuals to positive values (fewer constituents) while the background fluctuations induce a negative shift. For *LeSub*, the distributions in PYTHIA and PYTHIA embedded simulations are similar due to the resilience of the observable to background fluctuations.

The right panels of Fig. 4 show the resolution of the shapes, quantified as the standard deviation σ of the distribution of residuals, as a function of the shape at particle level for pp and Pb–Pb collisions. At low angularity, the resolution is poor because these jets are more collimated and typically have fewer constituents. In this region, this shape is thus more sensitive to tracking inefficiency and background fluctuations. At higher angularities the resolution improves up to 20%. The resolution of $p_T D$ is overall below 15% and improves for harder jets when $p_T D$ approaches unity. A similar case holds for *LeSub*, for which the resolution improves at higher values of the shape and worsens at low values where detector effects have a larger impact.

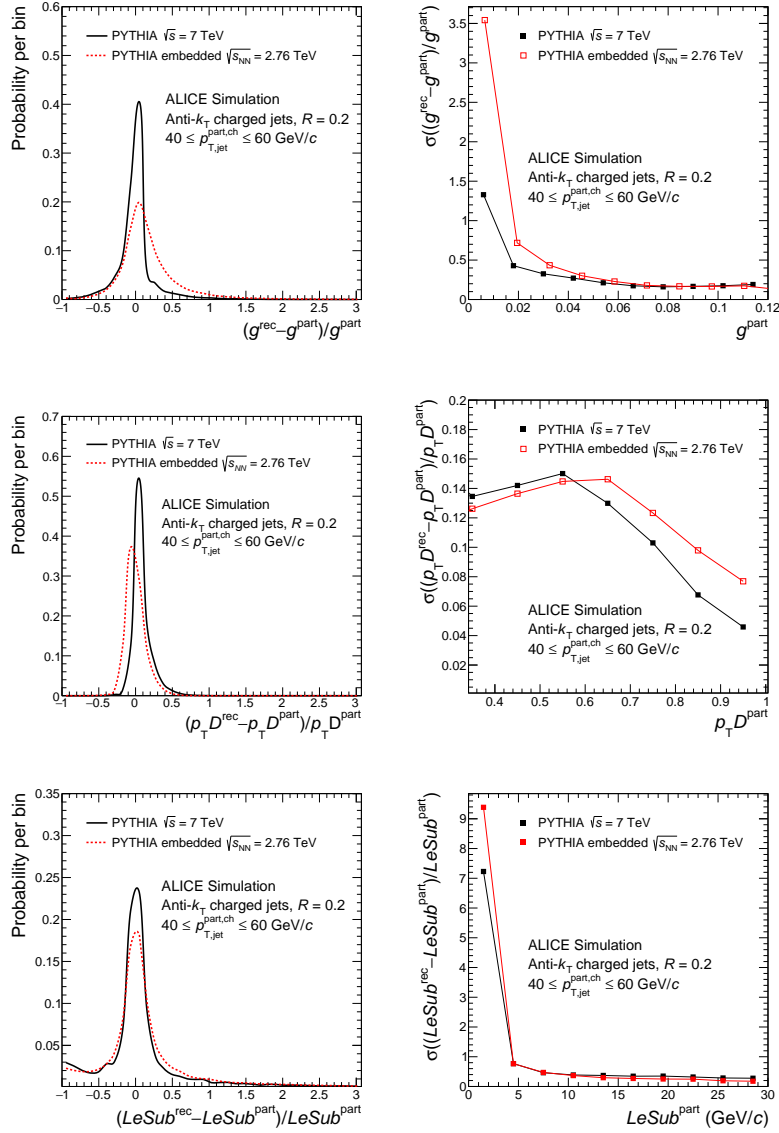


Fig. 4: Left plots show the distributions of residuals for the set of three jet shapes in a given interval of $p_{T,jet}^{part, ch}$ 40–60 GeV/c using the PYTHIA and PYTHIA embedded simulations. Right plots show the width (quantified as the standard deviation) of the distributions on the left as a function of the values of the shapes at particle level. The black and red curves correspond to pp and Pb–Pb simulations, respectively. The line connecting the points on the right is drawn to guide the eye.

7 Two-dimensional unfolding procedure

Residual background fluctuations and detector effects were unfolded to simultaneously correct the reconstructed jet transverse momentum and shape distributions back to the particle level. Bayesian unfolding in two dimensions as implemented in the RooUnfold package [39] was used. Several considerations needed to be taken into account. The 2D correlation $(p_{T,jet}^{rec, ch}, shape_{jet}^{rec, ch})$, which is the input to the unfolding, was binned such that there are at least 10 counts per bin, to guarantee statistical stability of the correction procedure, which also sets the upper limit of the input $p_{T,jet}^{rec, ch}$ range (80 GeV/c both in pp and Pb–Pb collisions). The shape input ranges are 0.3–1, 0.02–0.12, and 0–30 GeV/c for g , $p_T D$ and $LeSub$, respectively, for both collision systems. The raw input correlation should not contain combinatorial background, which was suppressed by truncating it at sufficiently high values of $p_{T,jet}^{rec, ch}$. The lower

limit of the input $p_{T,\text{jet}}^{\text{rec, ch}}$ range for unfolding in Pb–Pb collisions is 30 GeV/ c . As argued in Section 4, fake jet contamination above this limit for jets measured with $R = 0.2$ is negligible. In pp collisions, the cutoff is set at $p_{T,\text{jet}}^{\text{rec, ch}} = 20$ GeV/ c .

The particle-level $p_{T,\text{jet}}^{\text{part, ch}}$ range of the response matrix is from 0 to 200 GeV/ c . The shape ranges at the particle level are 0–1, 0–0.12 and 0–50 GeV/ c for g , $p_T D$, and $LeSub$, respectively. The particle-level ranges were extended beyond the input ranges to allow for jet migration into the reconstructed level range due to background fluctuations and tracking efficiency losses. When the data input is truncated, feed-in from detector-level jets outside the truncated range had to be considered and corrected for. However, this correction (referred to as kinematic efficiency) is purely based on MC and has to be limited by considering unfolded bins far away from the truncation thresholds. Thus, our final results are presented for the jet momentum interval 40–60 GeV/ c .

We tested the stability of the unfolding by refolding the solution back and checking the agreement with the raw distribution. In pp (Pb–Pb) collisions, both distributions agree within 1% (5%) after the second (third) iteration. The unfolding solutions converged after few iterations (note that convergence occurs globally in 2D and not just in a given interval of jet p_T). We also performed a closure test, where two statistically independent MC samples are used to fill the response and the pseudo-data. In this case, the unfolded solution agrees with the MC truth within less than 10% in pp and Pb–Pb collisions.

8 Systematic uncertainties

The systematic uncertainties for the shapes were determined by varying the analysis settings for instrumental response and background fluctuations. The systematic uncertainties are listed below:

- Tracking efficiency uncertainty for the used track selection is $\pm 4\%$ and this was used as source to estimate the jet energy scale uncertainty [16].
- The prior in the 2D Bayesian implementation of RooUnfold was taken as the projection of the response matrix onto the true axes. The default prior was PYTHIA Perugia 0. We considered three different variations. As the systematic uncertainty in a given bin we take the maximal deviation out of the three variations. The first variation was to re-weight the response matrix such that the prior coincides with the unfolding solution. The second considered variation was obtained by re-weighting the response matrix such that the projection onto true axis was that of purely gluonic jets. The third variation was obtained by re-weighting the response matrix such that the projection onto the true axis was that of purely quark jets.
- The regularization was given by the number of iterations considered, which was 4 (8) for pp (Pb–Pb) collisions in the default solutions. The uncertainty in the regularization was estimated by considering differences to solutions for one less and two more iterations.
- The minimum accepted jet $p_{T,\text{jet}}^{\text{ch}}$ as input to the unfolding was 20 (30) GeV/ c in pp (Pb–Pb) collisions. As a variation, we lowered the truncation by 10 GeV/ c .
- The binning of the raw input was changed arbitrarily (but keeping the statistical requirements of at least 10 counts per bin) in both the $p_{T,\text{jet}}^{\text{ch}}$ and shape dimensions.
- The choice of the background subtraction method in Pb–Pb collisions affected mostly the tails of the distribution and resulted in a variation of 10% at most.
- In Pb–Pb collisions, the matching criterion in the tagging algorithm was relaxed so that the response was filled with pairs of jets where the reconstructed embedded jet contained at least 40% of the probe jet momentum.

Shape	$p_T D$			g			$LeSub$ (GeV/c)		
	0.3-0.4	0.5-0.6	0.8-1	0-0.02	0.05-0.06	0.08-0.12	0-5	10-15	20-30
Tracking	10%	0.70%	11%	10%	1.7%	4.2%	1.8%	0.5%	6.6%
Prior	+0.3% -0.0%	+0.9% -0.0%	+0.0% -0.0%	+0.0% -3.0%	+0.0% -1.2%	+3.0% -0.0%	+0.9% -0.0%	+0.6% -0.0%	+0.5% -0.0%
Regularization	+0.1% -0.3%	+0.7% -1.2%	+0.4% -0.1%	+5.9% -2.7%	+2.3% -1.0%	+2.6% -4.5%	+0.8% -1.3%	+0.6% -0.6%	+0.6% -0.0%
Truncation	+0.0% -0.7%	+0.0% -0.1%	+0.5% -0.0%	+0.3% -0.0%	+0.0% -0.2%	+0.3% -0.0%	+0.1% -0.0%	+0.0% -0.1%	+0.1% -0.0%
Binning	1.4%	1.6%	4.2%	0.2%	6.4%	2.5%	2.1%	1.8%	0.9%
Total	+10% -10%	+2.1% -2.2%	+11% -11%	+12% -11%	+7.0% -6.8%	+6.3% -6.7%	+3.0% -3.1%	+2.1% -2.0%	+6.7% -6.6%

Table 1: Relative systematic uncertainties on the measured jet shapes in pp collisions for three selected jet shape intervals in the jet $p_{T,jet}^{ch}$ range of 40–60 GeV/c.

Shape	$p_T D$			g			$LeSub$ (GeV/c)		
	0.3-0.4	0.5-0.6	0.8-1	0-0.02	0.05-0.06	0.08-0.12	0-5	10-15	20-30
Tracking	0.7%	1.1%	3.3%	9.6%	2.9%	4.9%	0.6%	1.7%	0.8%
Prior	20%	2.6%	7.4%	7.6%	8.1%	20%	7.5%	7.9%	9.0%
Regularization	+0.6% -1.5%	+0.3% -0.8%	+0.1% -0.3%	+0.3% -0.9%	+0.5% -0.8%	+0.1% -0.0%	+0.4% -1.1%	+0.2% -0.1%	+4.3% -1.7%
Truncation	+0.0% -18%	+1.6% -0.0%	+3.9% -0.0%	+3.7% -0.0%	+0.0% -1.0%	+0.0% -39%	+0.0% -25%	+10% -0.0%	+18% -0.0%
Binning	1.3%	2.3%	4.2%	2.3%	3.6%	3.5%	0.9%	7.9%	3.4%
Bkg.Sub	+5.5% -0.0%	+0.0% -2.1%	+0.0% -0.3%	+0.0% -2.5%	+0.0% -9.5%	+0.0% -13%	+0.0% -1.0%	+0.0% -6.7%	+0.0% -1.6%
Matching	+0.0% -0.5%	+0.2% -0.0%	+9.4% -0.0%	+2.6% -0.0%	+1.9% -0.0%	+23% -0.0%	+0.0% -4.3%	+0.0% -0.3%	+0.0% -0.7%
Total	+21% -27%	+4.0% -4.3%	+14% -9.2%	+13% -13%	+9.5% -13%	+31% -47%	+7.6% -26%	+15% -13%	+21% -10%

Table 2: Relative systematic uncertainties on the measured jet shapes in Pb–Pb collisions for three selected jet shape intervals in the jet $p_{T,jet}^{ch}$ range 40–60 GeV/c.

The different components of the systematic uncertainties for the different shapes are summarized in Tables 1 and 2 for pp and Pb–Pb collisions, respectively. The largest contribution to the systematic uncertainties on the fully corrected pp data comes from the tracking efficiency uncertainty, yet the total systematic uncertainty is smaller when compared to the statistical one. In Pb–Pb collisions, systematic uncertainties due to prior and subtraction method choice dominate over statistical uncertainties. All the uncertainties induce changes in the shape of our observables and the applied normalization causes long range anti-correlations. The total uncertainty is obtained by adding the different components in quadrature.

9 Results and discussion

Figure 5 presents the fully corrected jet shape distributions measured in pp collisions at $\sqrt{s} = 7$ TeV in the jet p_T range 40–60 GeV/c. The results are compared to PYTHIA Perugia 2011 and PYTHIA 8 tune 4C jet shape distributions obtained at the same collision energy. The ratio plots in the lower panels indicate a reasonable agreement within 20%. Large non-perturbative effects are expected for small- R jets [40] and seem to be well accounted for by the simulations.

Figure 6 shows the fully corrected jet shape distributions in Pb–Pb collisions at $\sqrt{s_{NN}} = 2.76$ TeV compared to PYTHIA Perugia 2011 and PYTHIA 8 tune 4C at the same collision energy and in the same jet p_T range of 40–60 GeV/c. The radial moment (upper left plot) appears to be shifted to lower values in

the measured data compared to PYTHIA. The $p_T D$ (upper right plot) is shifted to higher values in the measured data compared to PYTHIA. *LeSub* (bottom) shows no indication of modifications relative to PYTHIA. These results indicate that the fragmentation in Pb–Pb collisions is harder and more collimated than in vacuum at the same reconstructed energy.

The observed hardening of the fragmentation is qualitatively consistent with the observed enhancement of the high- z component of the fragmentation functions of inclusive jets measured by ATLAS and CMS in Pb–Pb collisions [11, 12]. More recent measurements of fragmentation functions of jets recoiling from photons at CMS [41] do not show an enhancement at high- z but rather indicate a depletion of the high- z component accompanied by an enhancement of the soft modes. When the jet fragmentation is studied as a function of the photon energy in gamma-jet events, where the transverse momentum of the photon balances the initial parton momentum from the hard scattering to good approximation, there is no bias towards higher Q^2 in Pb–Pb relative to pp compared to the case when the recoiling jet energy is used. To quantitatively compare the different observables that select different samples of jets (inclusive vs recoil) and that are subject to different kinematic cuts, modeling within the same theoretical framework is required.

In Fig. 7 we compared quark and gluon vacuum jet shape distributions from PYTHIA to our data. Since quark-initiated jets radiate less, their fragmentation is harder and less broad. Gluon-initiated jets can be thought of as an approximation to modified jets in the hypothetical case where quenching accelerates the shower evolution just by increasing the number of splittings. This scenario would lead to a broadening and softening of the in-cone shower (see differences in the shape between inclusive jets and gluon jets in the plot) as opposed to the data. The comparison in Fig. 7 indicates that the Pb–Pb fragmentation agrees more with a vacuum quark-like fragmentation than with a vacuum gluon-like fragmentation. It is worth noting that in the case where gluon jets interact more strongly with the medium than quark jets, their relative fractions might change for a given jet p_T in favour of more quark-initiated jets. In line with this argument, the simple toy model calculations described in Ref. [42] can explain qualitatively some aspects of the data like the hardening of the fragmentation function and p_T dependence of the jet suppression, just by using a varying quark fraction and a greater quenching for gluon jets.

Another ingredient that might contribute to the observed differences between jet shapes in Pb–Pb and pp collisions at the same $p_{T,\text{jet}}^{\text{ch}}$ is that the original energy of the parton initiating the jet shower is different in both systems. The significant suppression of jet rates at high p_T , $R_{AA} < 1$, suggests that the jet energy that is reconstructed in Pb–Pb collisions is smaller than the original parton energy; this could lead to a larger virtuality of jets in Pb–Pb than in pp collisions for a given momentum. Let's consider the case where a fraction $X\%$ of the jet momentum is lost coherently, meaning that the jet substructure is not resolved by the medium and the jet radiates as a single colour charge [2]. Since g and $p_T D$ are normalized to the jet p_T , a simple rescaling by a momentum fraction $X\%$ of each jet constituent leaves Eqs. 3 and 2 unmodified. In this scenario, the modified jet shapes, for a given reconstructed jet p_T , are simply the vacuum-like shapes of jets with a momentum higher by a fraction $1/(1 - X\%)$. As seen in Fig. 2, both g and $p_T D$ decrease with jet momentum in vacuum. Our experimental results show that the g distribution shifts to lower values in Pb–Pb collisions relative to the vacuum-like one. The $p_T D$ distribution, instead, increases, contrary to what is expected from a fully coherent energy loss scenario. Following these considerations, the medium seems to be able to resolve the jet structure at angular scales below $R = 0.2$.

We also compared our results to JEWEL calculations [43], which is a perturbative framework for jet evolution in the presence of a dense medium. The detailed description of the jet-medium interaction includes elastic scattering off medium constituents, inelastic medium-induced gluon radiation, and medium recoil. The medium recoil refers to the response of the medium to the jet. This component is a correlated background that cannot be experimentally suppressed. An extensive comparison of the model to the existing jet shapes was done (see Ref. [17]), showing that the contribution of the medium recoil to

the modification of the jet shapes is large, in particular in those shapes that are most sensitive to the soft, large-angle quanta such as the jet mass or the subjet momentum imbalance z_g . Figure 8 shows the measured jet shape distributions compared to JEWEL calculations. The effects of the medium recoil are small, as expected for the small considered R and thus the measurement constrains the purely radiative aspects of the JEWEL shower modification. There is good agreement between the model and the data.

The ALICE measurement of the jet mass [16] for jets of $R = 0.4$ showed some hints of a reduction relative to the vacuum reference. The jet mass, as discussed in Section 2, differs parametrically from the angularity only in the power of the angle dependence, so it is also sensitive to the broadening or collimation of the jet shower. Comparisons to JEWEL revealed that the effect of jet mass reduction due to energy loss is obscured by the broadening due to the medium response or recoil [17], which contributes more strongly to jets with $R = 0.4$ than to the jet core measurements with $R = 0.2$ reported here.

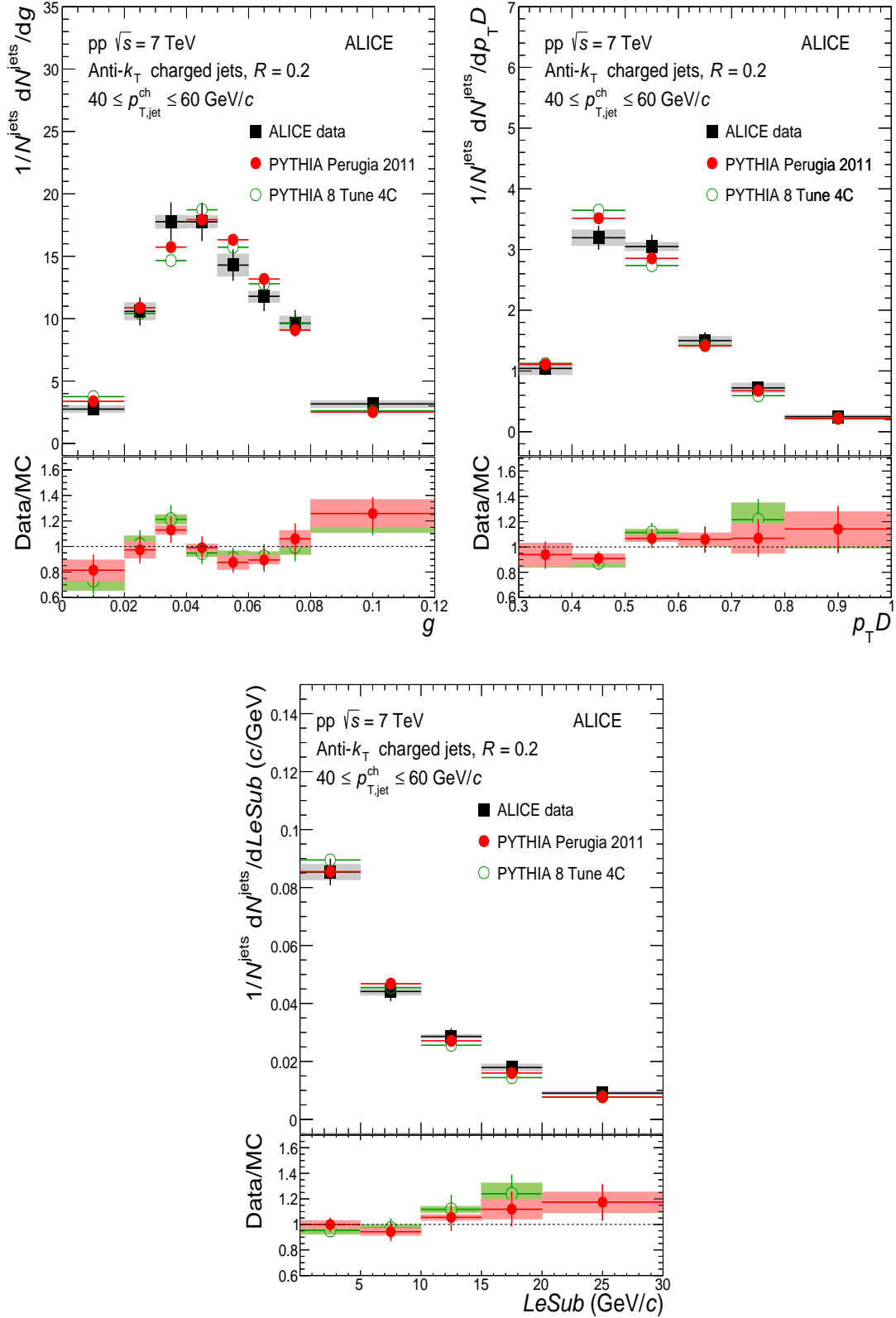


Fig. 5: Fully corrected jet shape distributions measured in pp collisions at $\sqrt{s} = 7$ TeV for $R = 0.2$ in the range of jet $p_{T,\text{jet}}^{\text{ch}}$ of 40–60 GeV/c. The results are compared to PYTHIA. The results are compared to PYTHIA. The coloured boxes represent the uncertainty on the jet shape (upper panels) and its propagation to the ratio (lower panels)

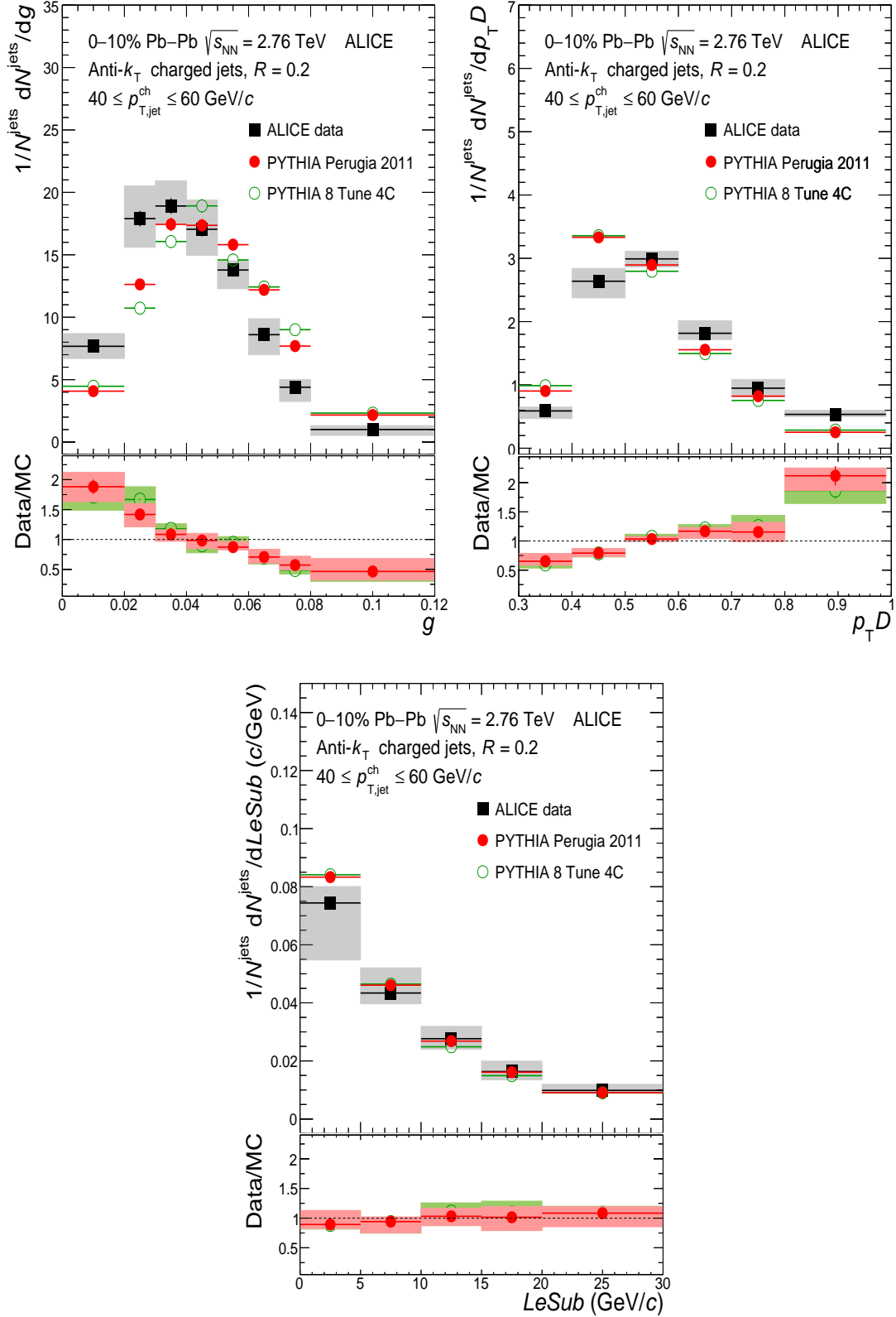


Fig. 6: Fully corrected jet shape distributions in 0–10% central Pb–Pb collisions at $\sqrt{s_{\text{NN}}} = 2.76$ TeV for $R = 0.2$ in the range of jet $p_{\text{T,jet}}^{\text{ch}}$ of 40–60 GeV/c. The results are compared to PYTHIA. The coloured boxes represent the uncertainty on the jet shape (upper panels) and its propagation to the ratio (lower panels).

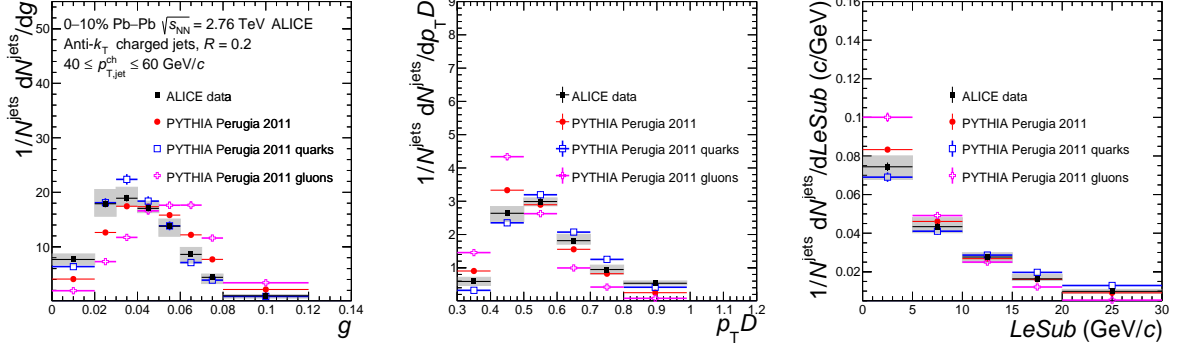


Fig. 7: Jet shape distributions in 0–10% central Pb–Pb collisions at $\sqrt{s_{\text{NN}}} = 2.76$ TeV for $R = 0.2$ in range of jet $p_{\text{T,jet}}^{\text{ch}}$ of 40–60 GeV/c compared to quark and gluon vacuum generated jet shape distributions. The coloured boxes represent the experimental uncertainty on the jet shapes.

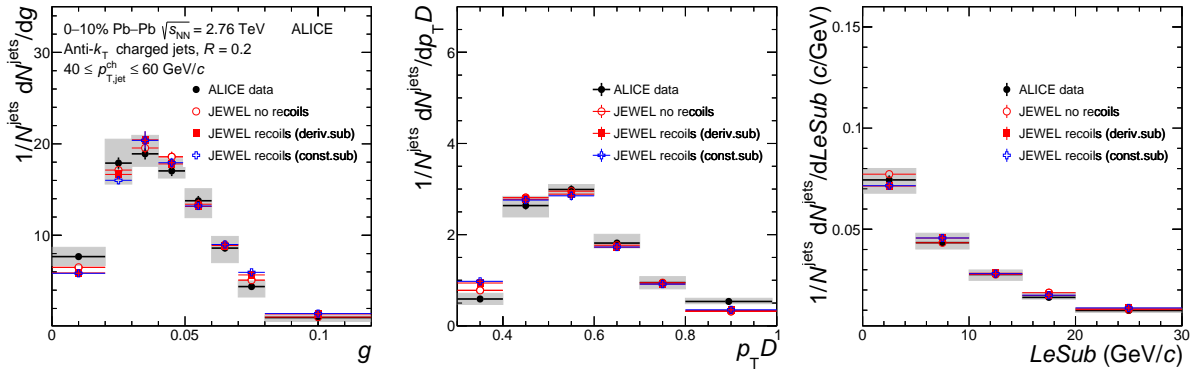


Fig. 8: Jet shape distributions in 0–10% central Pb–Pb collisions at $\sqrt{s_{\text{NN}}} = 2.76$ TeV for $R = 0.2$ in range of jet $p_{\text{T,jet}}^{\text{ch}}$ of 40–60 GeV/c compared to JEWEL with and without recoils with different subtraction methods. The coloured boxes represent the experimental uncertainty on the jet shapes.

10 Conclusions

In this paper, the first measurement of a new set of track-based jet shape distributions has been presented. The measurements were performed in pp collisions at $\sqrt{s} = 7$ TeV and in 0–10% central Pb–Pb collisions at $\sqrt{s_{NN}} = 2.76$ TeV in the low jet transverse momentum interval $40 \leq p_{T,\text{jet}}^{\text{ch}} \leq 60$ GeV/ c and using small jet resolution $R = 0.2$. The full correction to particle level and the measurement of an unbiased sample of jets with a constituent cutoff of 0.15 GeV/ c are key aspects of the analysis that allow exploring possible medium modifications in a wide dynamical range including soft modes.

The jet shapes reported here probe complementary aspects of the jet fragmentation and are used to test possible scenarios and ingredients of the theoretical description of jet quenching.

The measurements of g , $p_T D$, and $LeSub$ in pp collisions are within 20% in agreement with PYTHIA Perugia 2011 and PYTHIA 8 4C tunes.

In central Pb–Pb collisions, the measurements of g and $p_T D$ show that the jet core is more collimated and fragments harder than in pp collisions. The picture is qualitatively consistent with a more quark-like jet fragmentation, suggesting e.g. either a modified fragmentation pattern of all jets or a selection on quark-like jet properties imposed by the medium for these observables.

The role of colour coherence in the jet-medium interactions and the scales at which it dominates is a key ingredient in the characterisation of the medium. We argue that the medium-modification of g and $p_T D$ is not consistent with the scenario where the jets interact with the medium coherently, as single colour charges. This suggests that the medium is able to resolve the jet structure at angular scales smaller than $R = 0.2$.

Comparison to calculations using the JEWEL jet quenching model shows that the contribution of the medium response to the small-radius jets reported here is small and thus the data can constrain the effects due to energy loss, contrary to other measurements at larger R where the medium recoil can obscure the radiative effects.

Acknowledgements

The ALICE Collaboration would like to thank all its engineers and technicians for their invaluable contributions to the construction of the experiment and the CERN accelerator teams for the outstanding performance of the LHC complex. The ALICE Collaboration gratefully acknowledges the resources and support provided by all Grid centres and the Worldwide LHC Computing Grid (WLCG) collaboration. The ALICE Collaboration acknowledges the following funding agencies for their support in building and running the ALICE detector: A. I. Alikhanyan National Science Laboratory (Yerevan Physics Institute) Foundation (ANSL), State Committee of Science and World Federation of Scientists (WFS), Armenia; Austrian Academy of Sciences and Nationalstiftung für Forschung, Technologie und Entwicklung, Austria; Ministry of Communications and High Technologies, National Nuclear Research Center, Azerbaijan; Conselho Nacional de Desenvolvimento Científico e Tecnológico (CNPq), Universidade Federal do Rio Grande do Sul (UFRGS), Financiadora de Estudos e Projetos (Finep) and Fundação de Amparo à Pesquisa do Estado de São Paulo (FAPESP), Brazil; Ministry of Science & Technology of China (MSTC), National Natural Science Foundation of China (NSFC) and Ministry of Education of China (MOEC), China; Ministry of Science and Education, Croatia; Ministry of Education, Youth and Sports of the Czech Republic, Czech Republic; The Danish Council for Independent Research — Natural Sciences, the Carlsberg Foundation and Danish National Research Foundation (DNRF), Denmark; Helsinki Institute of Physics (HIP), Finland; Commissariat à l’Energie Atomique (CEA) and Institut National de Physique Nucléaire et de Physique des Particules (IN2P3) and Centre National de la Recherche Scientifique (CNRS), France; Bundesministerium für Bildung, Wissenschaft, Forschung und Technologie (BMBF) and GSI Helmholtzzentrum für Schwerionenforschung GmbH, Germany; General Secretariat

for Research and Technology, Ministry of Education, Research and Religions, Greece; National Research, Development and Innovation Office, Hungary; Department of Atomic Energy Government of India (DAE), Department of Science and Technology, Government of India (DST), University Grants Commission, Government of India (UGC) and Council of Scientific and Industrial Research (CSIR), India; Indonesian Institute of Science, Indonesia; Centro Fermi - Museo Storico della Fisica e Centro Studi e Ricerche Enrico Fermi and Istituto Nazionale di Fisica Nucleare (INFN), Italy; Institute for Innovative Science and Technology, Nagasaki Institute of Applied Science (IIST), Japan Society for the Promotion of Science (JSPS) KAKENHI and Japanese Ministry of Education, Culture, Sports, Science and Technology (MEXT), Japan; Consejo Nacional de Ciencia (CONACYT) y Tecnología, through Fondo de Cooperación Internacional en Ciencia y Tecnología (FONCICYT) and Dirección General de Asuntos del Personal Académico (DGAPA), Mexico; Nederlandse Organisatie voor Wetenschappelijk Onderzoek (NWO), Netherlands; The Research Council of Norway, Norway; Commission on Science and Technology for Sustainable Development in the South (COMSATS), Pakistan; Pontificia Universidad Católica del Perú, Peru; Ministry of Science and Higher Education and National Science Centre, Poland; Korea Institute of Science and Technology Information and National Research Foundation of Korea (NRF), Republic of Korea; Ministry of Education and Scientific Research, Institute of Atomic Physics and Romanian National Agency for Science, Technology and Innovation, Romania; Joint Institute for Nuclear Research (JINR), Ministry of Education and Science of the Russian Federation and National Research Centre Kurchatov Institute, Russia; Ministry of Education, Science, Research and Sport of the Slovak Republic, Slovakia; National Research Foundation of South Africa, South Africa; Centro de Aplicaciones Tecnológicas y Desarrollo Nuclear (CEADEN), Cubaenergía, Cuba and Centro de Investigaciones Energéticas, Medioambientales y Tecnológicas (CIEMAT), Spain; Swedish Research Council (VR) and Knut & Alice Wallenberg Foundation (KAW), Sweden; European Organization for Nuclear Research, Switzerland; National Science and Technology Development Agency (NSDTA), Suranaree University of Technology (SUT) and Office of the Higher Education Commission under NRU project of Thailand, Thailand; Turkish Atomic Energy Agency (TAEK), Turkey; National Academy of Sciences of Ukraine, Ukraine; Science and Technology Facilities Council (STFC), United Kingdom; National Science Foundation of the United States of America (NSF) and United States Department of Energy, Office of Nuclear Physics (DOE NP), United States of America.

References

- [1] A. Kurkela and U. A. Wiedemann, “Picturing perturbative parton cascades in QCD matter,” *Phys. Lett.* **B740** (2015) 172–178, arXiv:1407.0293 [hep-ph].
- [2] J. Casalderrey-Solana, Y. Mehtar-Tani, C. A. Salgado, and K. Tywoniuk, “New picture of jet quenching dictated by color coherence,” *Phys. Lett.* **B725** (2013) 357–360, arXiv:1210.7765 [hep-ph].
- [3] F. D’Eramo, M. Lekaveckas, H. Liu, and K. Rajagopal, “Momentum Broadening in Weakly Coupled Quark-Gluon Plasma (with a view to finding the quasiparticles within liquid quark-gluon plasma),” *JHEP* **05** (2013) 031, arXiv:1211.1922 [hep-ph].
- [4] G. P. Salam, “Towards Jetography,” *Eur. Phys. J.* **C67** (2010) 637–686, arXiv:0906.1833 [hep-ph].
- [5] ALICE Collaboration, B. Abelev *et al.*, “Measurement of the inclusive differential jet cross section in pp collisions at $\sqrt{s} = 2.76$ TeV,” *Phys. Lett.* **B722** (2013) 262–272, arXiv:1301.3475 [nucl-ex].
- [6] CMS Collaboration, S. Chatrchyan *et al.*, “Measurement of the ratio of inclusive jet cross sections using the anti- k_T algorithm with radius parameters $R=0.5$ and 0.7 in pp collisions at $\sqrt{s} = 7$ TeV,” arXiv:1406.0324 [hep-ex].
- [7] M. Dasgupta, F. A. Dreyer, G. P. Salam, and G. Soyez, “Inclusive jet spectrum for small-radius

- jets,” *JHEP* **06** (2016) 057, arXiv:1602.01110 [hep-ph].
- [8] ATLAS Collaboration, G. Aad *et al.*, “Measurement of the jet radius and transverse momentum dependence of inclusive jet suppression in lead-lead collisions at $\sqrt{s_{\text{NN}}} = 2.76$ TeV with the ATLAS detector,” *Phys. Lett.* **B719** (2013) 220–241, arXiv:1208.1967 [hep-ex].
- [9] ALICE Collaboration, B. Abelev *et al.*, “Measurement of charged jet suppression in Pb–Pb collisions at $\sqrt{s_{\text{NN}}} = 2.76$ TeV,” *JHEP* **03** (2014) 013, arXiv:1311.0633 [nucl-ex].
- [10] ALICE Collaboration, J. Adam *et al.*, “Measurement of jet quenching with semi-inclusive hadron-jet distributions in central Pb–Pb collisions at $\sqrt{s_{\text{NN}}} = 2.76$ TeV,” *JHEP* **09** (2015) 170, arXiv:1506.03984 [nucl-ex].
- [11] ATLAS Collaboration, M. Aaboud *et al.*, “Measurement of jet fragmentation in Pb+Pb and pp collisions at $\sqrt{s_{\text{NN}}} = 2.76$ TeV with the ATLAS detector at the LHC,” *Eur. Phys. J.* **C77** (2017) 379, arXiv:1702.00674 [hep-ex].
- [12] CMS Collaboration, S. Chatrchyan *et al.*, “Measurement of jet fragmentation in PbPb and pp collisions at $\sqrt{s_{\text{NN}}} = 2.76$ TeV,” *Phys. Rev.* **C90** (2014) 024908, arXiv:1406.0932 [nucl-ex].
- [13] CMS Collaboration, V. Khachatryan *et al.*, “Measurement of transverse momentum relative to dijet systems in Pb–Pb and pp collisions at $\sqrt{s_{\text{NN}}} = 2.76$ TeV,” *JHEP* **01** (2016) 006, arXiv:1509.09029 [nucl-ex].
- [14] CMS Collaboration, C. Collaboration, “Jet-track correlations in Pb–Pb collisions at 2.76 TeV,” *CMS-PAS-HIN-14-016* (2015).
- [15] CMS Collaboration, S. Chatrchyan *et al.*, “Modification of jet shapes in Pb–Pb collisions at $\sqrt{s_{\text{NN}}} = 2.76$ TeV,” *Phys. Lett.* **B730** (2014) 243–263, arXiv:1310.0878 [nucl-ex].
- [16] ALICE Collaboration, S. Acharya *et al.*, “First measurement of jet mass in Pb–Pb and p–Pb collisions at the LHC,” *Phys. Lett.* **B776** (2018) 249–264, arXiv:1702.00804 [nucl-ex].
- [17] R. Kunnawalkam Elayavalli and K. C. Zapp, “Medium response in JEWEL and its impact on jet shape observables in heavy ion collisions,” *JHEP* **07** (2017) 141, arXiv:1707.01539 [hep-ph].
- [18] J. M. Butterworth, A. R. Davison, M. Rubin, and G. P. Salam, “Jet substructure as a new Higgs search channel at the LHC,” *Phys. Rev. Lett.* **100** (2008) 242001, arXiv:0802.2470 [hep-ph].
- [19] A. J. Larkoski, S. Marzani, G. Soyez, and J. Thaler, “Soft Drop,” *JHEP* **05** (2014) 146, arXiv:1402.2657 [hep-ph].
- [20] ALICE Collaboration, N. Zardoshti, “Investigating the Role of Coherence Effects on Jet Quenching in Pb–Pb Collisions at $\sqrt{s_{\text{NN}}} = 2.76$ TeV using Jet Substructure,” *Nucl. Phys.* **A967** (2017) 560–563, arXiv:1705.03383 [nucl-ex].
- [21] CMS Collaboration, A. M. Sirunyan *et al.*, “Measurement of the Splitting Function in pp and Pb-Pb Collisions at $\sqrt{s_{\text{NN}}} = 5.02$ TeV,” *Phys. Rev. Lett.* **120** no. 14, (2018) 142302, arXiv:1708.09429 [nucl-ex].
- [22] STAR Collaboration, K. Kauder, “Measurement of the Shared Momentum Fraction z_g using Jet Reconstruction in p+p and Au+Au Collisions with STAR,” *Nucl. Phys.* **A967** (2017) 516–519, arXiv:1704.03046 [nucl-ex].
- [23] A. J. Larkoski, J. Thaler, and W. J. Waalewijn, “Gaining (Mutual) Information about Quark/Gluon Discrimination,” *JHEP* **11** (2014) 129, arXiv:1408.3122 [hep-ph].
- [24] T. Sjostrand, S. Mrenna, and P. Z. Skands, “PYTHIA 6.4 Physics and Manual,” *JHEP* **05** (2006) 026, arXiv:hep-ph/0603175 [hep-ph].
- [25] ALICE Collaboration, K. Aamodt *et al.*, “The ALICE experiment at the CERN LHC,” *JINST* **3** (2008) S08002.
- [26] ALICE Collaboration, B. B. Abelev *et al.*, “Performance of the ALICE Experiment at the CERN LHC,” *Int. J. Mod. Phys.* **A29** (2014) 1430044, arXiv:1402.4476 [nucl-ex].
- [27] ALICE Collaboration, B. Abelev *et al.*, “Centrality Dependence of Charged Particle Production at

- Large Transverse Momentum in Pb–Pb Collisions at $\sqrt{s_{\text{NN}}} = 2.76$ TeV,” *Phys. Lett.* **B720** (2013) 52–62, arXiv:1208.2711 [hep-ex].
- [28] ALICE Collaboration, B. B. Abelev *et al.*, “Charged jet cross sections and properties in proton-proton collisions at $\sqrt{s} = 7$ TeV,” *Phys. Rev.* **D91** (2015) 112012, arXiv:1411.4969 [nucl-ex].
- [29] P. Z. Skands, “Tuning Monte Carlo Generators: The Perugia Tunes,” *Phys.Rev.* **D82** (2010) 074018, arXiv:1005.3457 [hep-ph].
- [30] R. Brun, F. Bruyant, M. Maire, A.C. McPherson, and P. Zancarini, “GEANT3 User’s Guide,” *CERN Data Handling Division DD/EE/84-1* (1985).
- [31] M. Cacciari, G. P. Salam, and G. Soyez, “The anti- k_t jet clustering algorithm,” *JHEP* **04** (2008) 063, arXiv:0802.1189 [hep-ph].
- [32] M. Cacciari, G. P. Salam, and G. Soyez, “FastJet User Manual,” *Eur.Phys.J.* **C72** (2012) 1896, arXiv:1111.6097 [hep-ph].
- [33] M. Cacciari, G. P. Salam, and G. Soyez, “The Catchment Area of Jets,” *JHEP* **04** (2008) 005, arXiv:0802.1188 [hep-ph].
- [34] G. de Barros, B. Fenton-Olsen, P. Jacobs, and M. Ploskon, “Data-driven analysis methods for the measurement of reconstructed jets in heavy ion collisions at RHIC and LHC,” *Nucl.Phys.* **A910-911** (2013) 314–318, arXiv:1208.1518 [hep-ex].
- [35] STAR Collaboration, P. M. Jacobs, “Background Fluctuations in Heavy Ion Jet Reconstruction,” *Nucl. Phys.* **A855** (2011) 299, arXiv:1012.2406 [nucl-ex].
- [36] G. Soyez, G. P. Salam, J. Kim, S. Dutta, and M. Cacciari, “Pileup subtraction for jet shapes,” *Phys. Rev. Lett.* **110** (2013) 162001, arXiv:1211.2811 [hep-ph].
- [37] P. Berta, M. Spousta, D. W. Miller, and R. Leitner, “Particle-level pileup subtraction for jets and jet shapes,” *JHEP* **06** (2014) 092, arXiv:1403.3108 [hep-ex].
- [38] ALICE Collaboration, B. Abelev *et al.*, “Measurement of Event Background Fluctuations for Charged Particle Jet Reconstruction in Pb–Pb collisions at $\sqrt{s_{\text{NN}}} = 2.76$ TeV,” *JHEP* **03** (2012) 053, arXiv:1201.2423 [hep-ex].
- [39] R. webpage <http://hepunix.rl.ac.uk/~adye/software/unfold/RooUnfold.html>.
- [40] M. Dasgupta, L. Magnea, and G. P. Salam, “Non-perturbative QCD effects in jets at hadron colliders,” *JHEP* **02** (2008) 055, arXiv:0712.3014 [hep-ph].
- [41] CMS Collaboration, A. M. Sirunyan *et al.*, “Observation of medium induced modifications of jet fragmentation in PbPb collisions using isolated-photon-tagged jets,” arXiv:1801.04895 [hep-ex].
- [42] M. Spousta and B. Cole, “Interpreting single jet measurements in Pb+Pb collisions at the LHC,” *Eur. Phys. J.* **C76** (2016) 50, arXiv:1504.05169 [hep-ph].
- [43] K. Zapp, G. Ingelman, J. Rathsman, J. Stachel, and U. A. Wiedemann, “A Monte Carlo Model for ‘Jet Quenching’,” *Eur. Phys. J.* **C60** (2009) 617–632, arXiv:0804.3568 [hep-ph].

A The ALICE Collaboration

S. Acharya¹³⁹, F.T.-. Acosta²⁰, D. Adamová⁹³, A. Adler⁷⁴, J. Adolfsson⁸⁰, M.M. Aggarwal⁹⁸, G. Aglieri Rinella³⁴, M. Agnello³¹, N. Agrawal⁴⁸, Z. Ahammed¹³⁹, S.U. Ahn⁷⁶, S. Aiola¹⁴⁴, A. Akindinov⁶⁴, M. Al-Turany¹⁰⁴, S.N. Alam¹³⁹, D.S.D. Albuquerque¹²¹, D. Aleksandrov⁸⁷, B. Alessandro⁵⁸, R. Alfaro Molina⁷², Y. Ali¹⁵, A. Alici^{10,27,53}, A. Alkin², J. Alme²², T. Alt⁶⁹, L. Altenkamper²², I. Altsybeev¹¹¹, M.N. Anaam⁶, C. Andrei⁴⁷, D. Andreou³⁴, H.A. Andrews¹⁰⁸, A. Andronic^{104,142}, M. Angeletti³⁴, V. Anguelov¹⁰², C. Anson¹⁶, T. Antičić¹⁰⁵, F. Antinori⁵⁶, P. Antonioli⁵³, R. Anwar¹²⁵, N. Apadula⁷⁹, L. Aphecetche¹¹³, H. Appelshäuser⁶⁹, S. Arcelli²⁷, R. Arnaldi⁵⁸, I.C. Arsene²¹, M. Arslandok¹⁰², A. Augustinus³⁴, R. Averbeck¹⁰⁴, M.D. Azmi¹⁷, A. Badalà⁵⁵, Y.W. Baek^{40,60}, S. Bagnasco⁵⁸, R. Bailhache⁶⁹, R. Bala⁹⁹, A. Baldisseri¹³⁵, M. Ball⁴², R.C. Baral⁸⁵, A.M. Barbano²⁶, R. Barbera²⁸, F. Barile⁵², L. Barioglio²⁶, G.G. Barnaföldi¹⁴³, L.S. Barnby⁹², V. Barret¹³², P. Bartalini⁶, K. Barth³⁴, E. Bartsch⁶⁹, N. Bastid¹³², S. Basu¹⁴¹, G. Batigne¹¹³, B. Batyunya⁷⁵, P.C. Batzing²¹, J.L. Bazo Alba¹⁰⁹, I.G. Bearden⁸⁸, H. Beck¹⁰², C. Bedda⁶³, N.K. Behera⁶⁰, I. Belikov¹³⁴, F. Bellini³⁴, H. Bello Martinez⁴⁴, R. Bellwied¹²⁵, L.G.E. Beltran¹¹⁹, V. Belyaev⁹¹, G. Bencedi¹⁴³, S. Beole²⁶, A. Bercuci⁴⁷, Y. Berdnikov⁹⁶, D. Berenyi¹⁴³, R.A. Bertens¹²⁸, D. Berzano^{34,58}, L. Betev³⁴, P.P. Bhaduri¹³⁹, A. Bhasin⁹⁹, I.R. Bhat⁹⁹, H. Bhatt⁴⁸, B. Bhattacharjee⁴¹, J. Bhom¹¹⁷, A. Bianchi²⁶, L. Bianchi¹²⁵, N. Bianchi⁵¹, J. Bielčič³⁷, J. Bielčiková⁹³, A. Bilandzic^{103,116}, G. Biro¹⁴³, R. Biswas³, S. Biswas³, J.T. Blair¹¹⁸, D. Blau⁸⁷, C. Blume⁶⁹, G. Boca¹³⁷, F. Bock³⁴, A. Bogdanov⁹¹, L. Boldizsár¹⁴³, M. Bombara³⁸, G. Bonomi¹³⁸, M. Bonora³⁴, H. Borel¹³⁵, A. Borissov^{102,142}, M. Borri¹²⁷, E. Botta²⁶, C. Bourjau⁸⁸, L. Bratrud⁶⁹, P. Braun-Munzinger¹⁰⁴, M. Bregant¹²⁰, T.A. Broker⁶⁹, M. Broz³⁷, E.J. Brucken⁴³, E. Bruna⁵⁸, G.E. Bruno^{33,34}, D. Budnikov¹⁰⁶, H. Buesching⁶⁹, S. Bufalino³¹, P. Buhler¹¹², P. Buncic³⁴, O. Busch^{1,131}, Z. Buthelezi⁷³, J.B. Butt¹⁵, J.T. Buxton⁹⁵, J. Cabala¹¹⁵, D. Caffarri⁸⁹, H. Caines¹⁴⁴, A. Caliva¹⁰⁴, E. Calvo Villar¹⁰⁹, R.S. Camacho⁴⁴, P. Camerini²⁵, A.A. Capon¹¹², W. Carena³⁴, F. Carnesecchi^{10,27}, J. Castillo Castellanos¹³⁵, A.J. Castro¹²⁸, E.A.R. Casula⁵⁴, C. Ceballos Sanchez⁸, S. Chandra¹³⁹, B. Chang¹²⁶, W. Chang⁶, S. Chapeland³⁴, M. Chartier¹²⁷, S. Chattopadhyay¹³⁹, S. Chattopadhyay¹⁰⁷, A. Chauvin²⁴, C. Cheshkov¹³³, B. Cheynis¹³³, V. Chibante Barroso³⁴, D.D. Chinellato¹²¹, S. Cho⁶⁰, P. Chochula³⁴, T. Chowdhury¹³², P. Christakoglou⁸⁹, C.H. Christensen⁸⁸, P. Christiansen⁸⁰, T. Chujo¹³¹, S.U. Chung¹⁸, C. Cicalo⁵⁴, L. Cifarelli^{10,27}, F. Cindolo⁵³, J. Cleymans¹²⁴, F. Colamaria⁵², D. Colella⁵², A. Collu⁷⁹, M. Colocci²⁷, M. Concas^{11,58}, G. Conesa Balbastre⁷⁸, Z. Conesa del Valle⁶¹, J.G. Contreras³⁷, T.M. Cormier⁹⁴, Y. Corrales Morales⁵⁸, P. Cortese³², M.R. Cosentino¹²², F. Costa³⁴, S. Costanza¹³⁷, J. Crkovská⁶¹, P. Crochet¹³², E. Cuautle⁷⁰, L. Cunqueiro^{94,142}, T. Dahms^{103,116}, A. Dainese⁵⁶, F.P.A. Damas^{113,135}, S. Dani⁶⁶, M.C. Danisch¹⁰², A. Danu⁶⁸, D. Das¹⁰⁷, I. Das¹⁰⁷, S. Das³, A. Dash⁸⁵, S. Dash⁴⁸, S. De⁴⁹, A. De Caro³⁰, G. de Cataldo⁵², C. de Conti¹²⁰, J. de Cuveland³⁹, A. De Falco²⁴, D. De Gruttola^{10,30}, N. De Marco⁵⁸, S. De Pasquale³⁰, R.D. De Souza¹²¹, H.F. Degenhardt¹²⁰, A. Deisting^{102,104}, A. Deloff⁸⁴, S. Delsanto²⁶, C. Deplano⁸⁹, P. Dhankeher⁴⁸, D. Di Bari³³, A. Di Mauro³⁴, B. Di Ruzza⁵⁶, R.A. Diaz⁸, T. Dietel¹²⁴, P. Dillenseger⁶⁹, Y. Ding⁶, R. Diviá³⁴, Ø. Djuvsland²², A. Dobrin³⁴, D. Domenicis Gimenez¹²⁰, B. Dönigus⁶⁹, O. Dordic²¹, A.K. Dubey¹³⁹, A. Dubla¹⁰⁴, L. Ducroux¹³³, S. Dudi⁹⁸, A.K. Duggal⁹⁸, M. Dukhishyam⁸⁵, P. Dupieux¹³², R.J. Ehlers¹⁴⁴, D. Elia⁵², E. Endress¹⁰⁹, H. Engel⁷⁴, E. Epple¹⁴⁴, B. Erazmus¹¹³, F. Erhardt⁹⁷, M.R. Ersdal²², B. Espagnon⁶¹, G. Eulisse³⁴, J. Eum¹⁸, D. Evans¹⁰⁸, S. Evdokimov⁹⁰, L. Fabbietti^{103,116}, M. Faggin²⁹, J. Faivre⁷⁸, A. Fantoni⁵¹, M. Fasel⁹⁴, L. Feldkamp¹⁴², A. Felicioli⁵⁸, G. Feofilov¹¹¹, A. Fernández Téllez⁴⁴, A. Ferretti²⁶, A. Festanti³⁴, V.J.G. Feuillard¹⁰², J. Figiel¹¹⁷, M.A.S. Figueredo¹²⁰, S. Filchagin¹⁰⁶, D. Finogeev⁶², F.M. Fionda²², G. Fiorenza⁵², F. Flor¹²⁵, M. Floris³⁴, S. Foertsch⁷³, P. Foka¹⁰⁴, S. Fokin⁸⁷, E. Fragiacomo⁵⁹, A. Francescon³⁴, A. Francisco¹¹³, U. Frankenfeld¹⁰⁴, G.G. Fronze²⁶, U. Fuchs³⁴, C. Furget⁷⁸, A. Furs⁶², M. Fusco Girard³⁰, J.J. Gaardhøje⁸⁸, M. Gagliardi²⁶, A.M. Gago¹⁰⁹, K. Gajdosova⁸⁸, M. Gallio²⁶, C.D. Galvan¹¹⁹, P. Ganoti⁸³, C. Garabatos¹⁰⁴, E. Garcia-Solis¹¹, K. Garg²⁸, C. Gargiulo³⁴, P. Gasik^{103,116}, E.F. Gauger¹¹⁸, M.B. Gay Ducati⁷¹, M. Germain¹⁰², J. Ghosh¹⁰⁷, P. Ghosh¹³⁹, S.K. Ghosh³, P. Gianotti⁵¹, P. Giubellino^{58,104}, P. Giubilato²⁹, P. Glässel¹⁰², D.M. Gómez Coral⁷², A. Gomez Ramirez⁷⁴, V. Gonzalez¹⁰⁴, P. González-Zamora⁴⁴, S. Gorbunov³⁹, L. Görlich¹¹⁷, S. Gotovac³⁵, V. Grabski⁷², L.K. Graczykowski¹⁴⁰, K.L. Graham¹⁰⁸, L. Greiner⁷⁹, A. Grelli⁶³, C. Grigoras³⁴, V. Grigoriev⁹¹, A. Grigoryan¹, S. Grigoryan⁷⁵, J.M. Gronefeld¹⁰⁴, F. Grosa³¹, J.F. Grosse-Oetringhaus³⁴, R. Grosso¹⁰⁴, R. Guernane⁷⁸, B. Guerzoni²⁷, M. Guittiere¹¹³, K. Gulbrandsen⁸⁸, T. Gunji¹³⁰, A. Gupta⁹⁹, R. Gupta⁹⁹, I.B. Guzman⁴⁴, R. Haake^{34,144}, M.K. Habib¹⁰⁴, C. Hadjidakis⁶¹, H. Hamagaki⁸¹, G. Hamar¹⁴³, M. Hamid⁶, J.C. Hamon¹³⁴, R. Hannigan¹¹⁸, M.R. Haque⁶³, A. Harlanderova¹⁰⁴, J.W. Harris¹⁴⁴, A. Harton¹¹, H. Hassan⁷⁸, D. Hatzifotiadou^{10,53}, S. Hayashi¹³⁰, S.T. Heckel⁶⁹, E. Hellbär⁶⁹, H. Helstrup³⁶, A. Hergelegiu⁴⁷, E.G. Hernandez⁴⁴, G. Herrera Corral⁹, F. Herrmann¹⁴², K.F. Hetland³⁶, T.E. Hilden⁴³, H. Hillemanns³⁴, C. Hills¹²⁷, B. Hippolyte¹³⁴, B. Hohlweger¹⁰³, D. Horak³⁷, S. Hornung¹⁰⁴, R. Hosokawa^{78,131}, J. Hota⁶⁶, P. Hristov³⁴, C. Huang⁶¹, C. Hughes¹²⁸, P. Huhn⁶⁹, T.J. Humanic⁹⁵, H. Hushnud¹⁰⁷, N. Hussain⁴¹, T. Hussain¹⁷, D. Hutter³⁹, D.S. Hwang¹⁹, J.P. Iddon¹²⁷, R. Ilkaev¹⁰⁶, M. Inaba¹³¹, M. Ippolitov⁸⁷, M.S. Islam¹⁰⁷, M. Ivanov¹⁰⁴,

V. Ivanov⁹⁶, V. Izucheev⁹⁰, B. Jacak⁷⁹, N. Jacazio²⁷, P.M. Jacobs⁷⁹, M.B. Jadhav⁴⁸, S. Jadlovska¹¹⁵, J. Jadlovska¹¹⁵, S. Jaelani⁶³, C. Jahnke^{116,120}, M.J. Jakubowska¹⁴⁰, M.A. Janik¹⁴⁰, C. Jena⁸⁵, M. Jercic⁹⁷, O. Jevons¹⁰⁸, R.T. Jimenez Bustamante¹⁰⁴, M. Jin¹²⁵, P.G. Jones¹⁰⁸, A. Jusko¹⁰⁸, P. Kalinak⁶⁵, A. Kalweit³⁴, J.H. Kang¹⁴⁵, V. Kaplin⁹¹, S. Kar⁶, A. Karasu Uysal⁷⁷, O. Karavichev⁶², T. Karavicheva⁶², P. Karczmarczyk³⁴, E. Karpechev⁶², U. Kebschull⁷⁴, R. Keidel⁴⁶, D.L.D. Keijdener⁶³, M. Keil³⁴, B. Ketzer⁴², Z. Khabanova⁸⁹, A.M. Khan⁶, S. Khan¹⁷, S.A. Khan¹³⁹, A. Khanzadeev⁹⁶, Y. Kharlov⁹⁰, A. Khatun¹⁷, A. Khuntia⁴⁹, M.M. Kielbowicz¹¹⁷, B. Kileng³⁶, B. Kim¹³¹, D. Kim¹⁴⁵, D.J. Kim¹²⁶, E.J. Kim¹³, H. Kim¹⁴⁵, J.S. Kim⁴⁰, J. Kim¹⁰², M. Kim^{60,102}, S. Kim¹⁹, T. Kim¹⁴⁵, T. Kim¹⁴⁵, K. Kindra⁹⁸, S. Kirsch³⁹, I. Kisel³⁹, S. Kiselev⁶⁴, A. Kisiel¹⁴⁰, J.L. Klay⁵, C. Klein⁶⁹, J. Klein⁵⁸, C. Klein-Bösing¹⁴², S. Klewin¹⁰², A. Kluge³⁴, M.L. Knichel³⁴, A.G. Knospe¹²⁵, C. Kobdaj¹¹⁴, M. Kofarago¹⁴³, M.K. Köhler¹⁰², T. Kollegger¹⁰⁴, N. Kondratyeva⁹¹, E. Kondratyuk⁹⁰, A. Konevskikh⁶², P.J. Konopka³⁴, M. Konyushikhin¹⁴¹, L. Koska¹¹⁵, O. Kovalenko⁸⁴, V. Kovalenko¹¹¹, M. Kowalski¹¹⁷, I. Králik⁶⁵, A. Kravčáková³⁸, L. Kreis¹⁰⁴, M. Krivda^{65,108}, F. Krizek⁹³, M. Krüger⁶⁹, E. Kryshen⁹⁶, M. Krzewicki³⁹, A.M. Kubera⁹⁵, V. Kučera^{60,93}, C. Kuhn¹³⁴, P.G. Kuijer⁸⁹, J. Kumar⁴⁸, L. Kumar⁹⁸, S. Kumar⁴⁸, S. Kundu⁸⁵, P. Kurashvili⁸⁴, A. Kurepin⁶², A.B. Kurepin⁶², S. Kuschpil⁹³, J. Kvapil¹⁰⁸, M.J. Kweon⁶⁰, Y. Kwon¹⁴⁵, S.L. La Pointe³⁹, P. La Rocca²⁸, Y.S. Lai⁷⁹, I. Lakomov³⁴, R. Langoy¹²³, K. Lapidus¹⁴⁴, A. Lardeux²¹, P. Larionov⁵¹, E. Laudi³⁴, R. Lavicka³⁷, R. Lea²⁵, L. Leardini¹⁰², S. Lee¹⁴⁵, F. Lehas⁸⁹, S. Lehner¹¹², J. Lehrbach³⁹, R.C. Lemmon⁹², I. León Monzón¹¹⁹, P. Lévai¹⁴³, X. Li¹², X.L. Li⁶, J. Lien¹²³, R. Lietava¹⁰⁸, B. Lim¹⁸, S. Lindal²¹, V. Lindenstruth³⁹, S.W. Lindsay¹²⁷, C. Lippmann¹⁰⁴, M.A. Lisa⁹⁵, V. Litichevskiy⁴³, A. Liu⁷⁹, H.M. Ljunggren⁸⁰, W.J. Llope¹⁴¹, D.F. Lodato⁶³, V. Loginov⁹¹, C. Loizides^{79,94}, P. Loncar³⁵, X. Lopez¹³², E. López Torres⁸, P. Luettig⁶⁹, J.R. Luhder¹⁴², M. Lunardon²⁹, G. Luparello⁵⁹, M. Lupi³⁴, A. Maevskaya⁶², M. Mager³⁴, S.M. Mahmood²¹, A. Maire¹³⁴, R.D. Majka¹⁴⁴, M. Malaev⁹⁶, Q.W. Malik²¹, L. Malinina^{III,75}, D. Mal'Kevich⁶⁴, P. Malzacher¹⁰⁴, A. Mamonov¹⁰⁶, V. Manko⁸⁷, F. Manso¹³², V. Manzari⁵², Y. Mao⁶, M. Marchionese^{129,133}, J. Mareš⁶⁷, G.V. Margagliotti²⁵, A. Margotti⁵³, J. Margutti⁶³, A. Marín¹⁰⁴, C. Markert¹¹⁸, M. Marquard⁶⁹, N.A. Martin^{102,104}, P. Martinengo³⁴, J.L. Martinez¹²⁵, M.I. Martínez⁴⁴, G. Martínez García¹¹³, M. Martinez Pedreira³⁴, S. Masciocchi¹⁰⁴, M. Maserà²⁶, A. Masoni⁵⁴, L. Massacrier⁶¹, E. Masson¹¹³, A. Mastroserio^{52,136}, A.M. Mathis^{103,116}, P.F.T. Matuoka¹²⁰, A. Matyja^{117,128}, C. Mayer¹¹⁷, M. Mazzilli³³, M.A. Mazzoni⁵⁷, F. Meddi²³, Y. Melikyan⁹¹, A. Menchaca-Rocha⁷², E. Meninno³⁰, J. Mercado Pérez¹⁰², M. Meres¹⁴, S. Mhlanga¹²⁴, Y. Miake¹³¹, L. Micheletti²⁶, M.M. Mieskolainen⁴³, D.L. Mihaylov¹⁰³, K. Mikhaylov^{64,75}, A. Mischke⁶³, A.N. Mishra⁷⁰, D. Miśkowiec¹⁰⁴, J. Mitra¹³⁹, C.M. Mitu⁶⁸, N. Mohammadi³⁴, A.P. Mohanty⁶³, B. Mohanty⁸⁵, M. Mohisin Khan^{IV,17}, D.A. Moreira De Godoy¹⁴², L.A.P. Moreno⁴⁴, S. Moretto²⁹, A. Morreale¹¹³, A. Morsch³⁴, T. Mrnjavac³⁴, V. Muccifora⁵¹, E. Mudnic³⁵, D. Mühlheim¹⁴², S. Muhuri¹³⁹, M. Mukherjee³, J.D. Mulligan¹⁴⁴, M.G. Munhoz¹²⁰, K. Mürning⁴², M.I.A. Muñoz⁷⁹, R.H. Munzer⁶⁹, H. Murakami¹³⁰, S. Murray⁷³, L. Musa³⁴, J. Musinsky⁶⁵, C.J. Myers¹²⁵, J.W. Myrcha¹⁴⁰, B. Naik⁴⁸, R. Nair⁸⁴, B.K. Nandi⁴⁸, R. Nania^{10,53}, E. Nappi⁵², A. Narayan⁴⁸, M.U. Naru¹⁵, A.F. Nassirpour⁸⁰, H. Natal da Luz¹²⁰, C. Nattrass¹²⁸, S.R. Navarro⁴⁴, K. Nayak⁸⁵, R. Nayak⁴⁸, T.K. Nayak¹³⁹, S. Nazarenko¹⁰⁶, R.A. Negrao De Oliveira^{34,69}, L. Nellen⁷⁰, S.V. Nesbo³⁶, G. Neskovic³⁹, F. Ng¹²⁵, M. Nicassio¹⁰⁴, J. Niedziela^{34,140}, B.S. Nielsen⁸⁸, S. Nikolaev⁸⁷, S. Nikulin⁸⁷, V. Nikulin⁹⁶, F. Noferini^{10,53}, P. Nomokonov⁷⁵, G. Nooren⁶³, J.C.C. Noris⁴⁴, J. Norman⁷⁸, A. Nyanin⁸⁷, J. Nystrand²², M. Ogino⁸¹, H. Oh¹⁴⁵, A. Ohlson¹⁰², J. Oleniacz¹⁴⁰, A.C. Oliveira Da Silva¹²⁰, M.H. Oliver¹⁴⁴, J. Onderwaater¹⁰⁴, C. Oppedisano⁵⁸, R. Orava⁴³, M. Oravec¹¹⁵, A. Ortiz Velasquez⁷⁰, A. Oskarsson⁸⁰, J. Otwinowski¹¹⁷, K. Oyama⁸¹, Y. Pachmayer¹⁰², V. Pacik⁸⁸, D. Pagano¹³⁸, G. Paic⁷⁰, P. Palni⁶, J. Pan¹⁴¹, S. Panebianco¹³⁵, V. Papikyan¹, P. Pareek⁴⁹, J. Park⁶⁰, J.E. Parkkila¹²⁶, S. Parmar⁹⁸, A. Passfeld¹⁴², S.P. Pathak¹²⁵, R.N. Patra¹³⁹, B. Paul⁵⁸, H. Pei⁶, T. Peitzmann⁶³, X. Peng⁶, L.G. Pereira⁷¹, H. Pereira Da Costa¹³⁵, D. Peresunko⁸⁷, E. Perez Lezama⁶⁹, V. Peskov⁶⁹, Y. Pestov⁴, V. Petráček³⁷, M. Petrovici⁴⁷, C. Petta²⁸, R.P. Pezzi⁷¹, S. Piano⁵⁹, M. Pika¹⁴, P. Pillot¹¹³, L.O.D.L. Pimentel⁸⁸, O. Pinazza^{34,53}, L. Pinsky¹²⁵, S. Pisano⁵¹, D.B. Piyarathna¹²⁵, M. Płoskoń⁷⁹, M. Planinic⁹⁷, F. Pliquett⁶⁹, J. Pluta¹⁴⁰, S. Pochybova¹⁴³, P.L.M. Podesta-Lerma¹¹⁹, M.G. Poghosyan⁹⁴, B. Polichtchouk⁹⁰, N. Poljak⁹⁷, W. Poonsawat¹¹⁴, A. Pop⁴⁷, H. Poppenborg¹⁴², S. Porteboeuf-Houssais¹³², V. Pozdniakov⁷⁵, S.K. Prasad³, R. Preghenella⁵³, F. Prino⁵⁸, C.A. Pruneau¹⁴¹, I. Pshenichnov⁶², M. Puccio²⁶, V. Punin¹⁰⁶, J. Putschke¹⁴¹, S. Raha³, S. Rajput⁹⁹, J. Rak¹²⁶, A. Rakotozafindrabe¹³⁵, L. Ramello³², F. Rami¹³⁴, R. Raniwala¹⁰⁰, S. Raniwala¹⁰⁰, S.S. Räsänen⁴³, B.T. Rascanu⁶⁹, R. Rath⁴⁹, V. Ratzka⁴², I. Ravasenga³¹, K.F. Read^{94,128}, K. Redlich^{V,84}, A. Rehman²², P. Reichelt⁶⁹, F. Reidt³⁴, X. Ren⁶, R. Renfordt⁶⁹, A. Reshetin⁶², J.-P. Revol¹⁰, K. Reygers¹⁰², V. Riabov⁹⁶, T. Richert^{63,80,88}, M. Richter²¹, P. Riedler³⁴, W. Riegler³⁴, F. Riggi²⁸, C. Ristea⁶⁸, S.P. Rode⁴⁹, M. Rodríguez Cahuantzi⁴⁴, K. Røed²¹, R. Rogalev⁹⁰, E. Rogochaya⁷⁵, D. Rohr³⁴, D. Röhrich²², P.S. Rokita¹⁴⁰, F. Ronchetti⁵¹, E.D. Rosas⁷⁰, K. Roslon¹⁴⁰, P. Rosnet¹³², A. Rossi^{29,56}, A. Rotondi¹³⁷, F. Roukoutakis⁸³, C. Roy¹³⁴, P. Roy¹⁰⁷, O.V. Rueda⁷⁰, R. Rui²⁵, B. Rumyantsev⁷⁵, A. Rustamov⁸⁶, E. Ryabinkin⁸⁷, Y. Ryabov⁹⁶, A. Rybicki¹¹⁷, S. Saarinen⁴³, S. Sadhu¹³⁹, S. Sadovskiy⁹⁰,

K. Šafařík³⁴, S.K. Saha¹³⁹, B. Sahoo⁴⁸, P. Sahoo⁴⁹, R. Sahoo⁴⁹, S. Sahoo⁶⁶, P.K. Sahu⁶⁶, J. Saini¹³⁹, S. Sakai¹³¹, M.A. Saleh¹⁴¹, S. Sambyal⁹⁹, V. Samsonov^{91,96}, A. Sandoval⁷², A. Sarkar⁷³, D. Sarkar¹³⁹, N. Sarkar¹³⁹, P. Sarma⁴¹, M.H.P. Sas⁶³, E. Scapparone⁵³, F. Scarlassara²⁹, B. Schaefer⁹⁴, H.S. Scheid⁶⁹, C. Schiaua⁴⁷, R. Schicker¹⁰², C. Schmidt¹⁰⁴, H.R. Schmidt¹⁰¹, M.O. Schmidt¹⁰², M. Schmidt¹⁰¹, N.V. Schmidt^{69,94}, J. Schukraft³⁴, Y. Schutz^{34,134}, K. Schwarz¹⁰⁴, K. Schweda¹⁰⁴, G. Scioli²⁷, E. Scomparin⁵⁸, M. Šefčík³⁸, J.E. Seger¹⁶, Y. Sekiguchi¹³⁰, D. Sekihata⁴⁵, I. Selyuzhenkov^{91,104}, S. Senyukov¹³⁴, E. Serradilla⁷², P. Sett⁴⁸, A. Sevcenco⁶⁸, A. Shabanov⁶², A. Shabetai¹¹³, R. Shahoyan³⁴, W. Shaikh¹⁰⁷, A. Shangaraev⁹⁰, A. Sharma⁹⁸, A. Sharma⁹⁹, M. Sharma⁹⁹, N. Sharma⁹⁸, A.I. Sheikh¹³⁹, K. Shigaki⁴⁵, M. Shimomura⁸², S. Shirinkin⁶⁴, Q. Shou^{6,110}, Y. Sibiriak⁸⁷, S. Siddhanta⁵⁴, K.M. Sielewicz³⁴, T. Siemiarczuk⁸⁴, D. Silvermyr⁸⁰, G. Simatovic⁸⁹, G. Simonetti^{34,103}, R. Singaraju¹³⁹, R. Singh⁸⁵, R. Singh⁹⁹, V. Singhal¹³⁹, T. Sinha¹⁰⁷, B. Sitar¹⁴, M. Sitta³², T.B. Skaali²¹, M. Slupecki¹²⁶, N. Smirnov¹⁴⁴, R.J.M. Snellings⁶³, T.W. Snellman¹²⁶, J. Sochan¹¹⁵, C. Soncco¹⁰⁹, J. Song¹⁸, A. Songmoolnak¹¹⁴, F. Soramel²⁹, S. Sorensen¹²⁸, F. Sozzi¹⁰⁴, I. Sputowska¹¹⁷, J. Stachel¹⁰², I. Stan⁶⁸, P. Stankus⁹⁴, E. Stenlund⁸⁰, D. Stocco¹¹³, M.M. Storetvedt³⁶, P. Strmen¹⁴, A.A.P. Suaide¹²⁰, T. Sugitate⁴⁵, C. Suire⁶¹, M. Suleymanov¹⁵, M. Suljic³⁴, R. Sultanov⁶⁴, M. Šumbera⁹³, S. Sumowidagdo⁵⁰, K. Suzuki¹¹², S. Swain⁶⁶, A. Szabo¹⁴, I. Szarka¹⁴, U. Tabassam¹⁵, J. Takahashi¹²¹, G.J. Tambave²², N. Tanaka¹³¹, M. Tarhini¹¹³, M.G. Tarzila⁴⁷, A. Tauro³⁴, G. Tejada Muñoz⁴⁴, A. Telesca³⁴, C. Terrevoli²⁹, B. Teyssier¹³³, D. Thakur⁴⁹, S. Thakur¹³⁹, D. Thomas¹¹⁸, F. Thoresen⁸⁸, R. Tieulent¹³³, A. Tikhonov⁶², A.R. Timmins¹²⁵, A. Toia⁶⁹, N. Topilskaya⁶², M. Toppi⁵¹, S.R. Torres¹¹⁹, S. Tripathy⁴⁹, S. Trogolo²⁶, G. Trombetta³³, L. Tropp³⁸, V. Trubnikov², W.H. Trzaska¹²⁶, T.P. Trzcinski¹⁴⁰, B.A. Trzeciak⁶³, T. Tsuji¹³⁰, A. Tumkin¹⁰⁶, R. Turrisi⁵⁶, T.S. Tveter²¹, K. Ullaland²², E.N. Umaka¹²⁵, A. Uras¹³³, G.L. Usai²⁴, A. Utrobicic⁹⁷, M. Vala¹¹⁵, L. Valencia Palomo⁴⁴, N. Valle¹³⁷, L.V.R. van Doremalen⁶³, J.W. Van Hoorne³⁴, M. van Leeuwen⁶³, P. Vande Vuyve³⁴, D. Varga¹⁴³, A. Vargas⁴⁴, M. Vargyas¹²⁶, R. Varma⁴⁸, M. Vasileiou⁸³, A. Vasiliev⁸⁷, A. Vauthier⁷⁸, O. Vázquez Doce^{103,116}, V. Vechernin¹¹¹, A.M. Veen⁶³, E. Vercellin²⁶, S. Vergara Limón⁴⁴, L. Vermunt⁶³, R. Vernet⁷, R. Vértesi¹⁴³, L. Vickovic³⁵, J. Viinikainen¹²⁶, Z. Vilakazi¹²⁹, O. Villalobos Baillie¹⁰⁸, A. Villatoro Tello⁴⁴, A. Vinogradov⁸⁷, T. Virgili³⁰, V. Vislavicius^{80,88}, A. Vodopyanov⁷⁵, M.A. Völkl¹⁰¹, K. Voloshin⁶⁴, S.A. Voloshin¹⁴¹, G. Volpe³³, B. von Haller³⁴, I. Vorobyev^{103,116}, D. Voscek¹¹⁵, D. Vranic^{34,104}, J. Vrláková³⁸, B. Wagner²², H. Wang⁶³, M. Wang⁶, Y. Watanabe¹³¹, M. Weber¹¹², S.G. Weber¹⁰⁴, A. Wegrzynek³⁴, D.F. Weiser¹⁰², S.C. Wenzel³⁴, J.P. Wessels¹⁴², U. Westerhoff¹⁴², A.M. Whitehead¹²⁴, J. Wiechula⁶⁹, J. Wikne²¹, G. Wilk⁸⁴, J. Wilkinson⁵³, G.A. Willems^{34,142}, M.C.S. Williams⁵³, E. Willsher¹⁰⁸, B. Windelband¹⁰², W.E. Witt¹²⁸, R. Xu⁶, S. Yalcin⁷⁷, K. Yamakawa⁴⁵, S. Yano^{45,135}, Z. Yin⁶, H. Yokoyama^{78,131}, I.-K. Yoo¹⁸, J.H. Yoon⁶⁰, V. Yurchenko², V. Zaccolo⁵⁸, A. Zaman¹⁵, C. Zampolli³⁴, H.J.C. Zanolli¹²⁰, N. Zardoshti¹⁰⁸, A. Zarochentsev¹¹¹, P. Závada⁶⁷, N. Zaviyalov¹⁰⁶, H. Zbroszczyk¹⁴⁰, M. Zhalov⁹⁶, X. Zhang⁶, Y. Zhang⁶, Z. Zhang^{6,132}, C. Zhao²¹, V. Zherebchevskii¹¹¹, N. Zhigareva⁶⁴, D. Zhou⁶, Y. Zhou⁸⁸, Z. Zhou²², H. Zhu⁶, J. Zhu⁶, Y. Zhu⁶, A. Zichichi^{10,27}, M.B. Zimmermann³⁴, G. Zinovjev², J. Zmeskal¹¹²

Affiliation Notes

^I Deceased

^{II} Also at: Dipartimento DET del Politecnico di Torino, Turin, Italy

^{III} Also at: M.V. Lomonosov Moscow State University, D.V. Skobeltsyn Institute of Nuclear, Physics, Moscow, Russia

^{IV} Also at: Department of Applied Physics, Aligarh Muslim University, Aligarh, India

^V Also at: Institute of Theoretical Physics, University of Wrocław, Poland

Collaboration Institutes

¹ A.I. Alikhanyan National Science Laboratory (Yerevan Physics Institute) Foundation, Yerevan, Armenia

² Bogolyubov Institute for Theoretical Physics, National Academy of Sciences of Ukraine, Kiev, Ukraine

³ Bose Institute, Department of Physics and Centre for Astroparticle Physics and Space Science (CAPSS), Kolkata, India

⁴ Budker Institute for Nuclear Physics, Novosibirsk, Russia

⁵ California Polytechnic State University, San Luis Obispo, California, United States

⁶ Central China Normal University, Wuhan, China

- ⁷ Centre de Calcul de l'IN2P3, Villeurbanne, Lyon, France
- ⁸ Centro de Aplicaciones Tecnológicas y Desarrollo Nuclear (CEADEN), Havana, Cuba
- ⁹ Centro de Investigación y de Estudios Avanzados (CINVESTAV), Mexico City and Mérida, Mexico
- ¹⁰ Centro Fermi - Museo Storico della Fisica e Centro Studi e Ricerche "Enrico Fermi", Rome, Italy
- ¹¹ Chicago State University, Chicago, Illinois, United States
- ¹² China Institute of Atomic Energy, Beijing, China
- ¹³ Chonbuk National University, Jeonju, Republic of Korea
- ¹⁴ Comenius University Bratislava, Faculty of Mathematics, Physics and Informatics, Bratislava, Slovakia
- ¹⁵ COMSATS Institute of Information Technology (CIIT), Islamabad, Pakistan
- ¹⁶ Creighton University, Omaha, Nebraska, United States
- ¹⁷ Department of Physics, Aligarh Muslim University, Aligarh, India
- ¹⁸ Department of Physics, Pusan National University, Pusan, Republic of Korea
- ¹⁹ Department of Physics, Sejong University, Seoul, Republic of Korea
- ²⁰ Department of Physics, University of California, Berkeley, California, United States
- ²¹ Department of Physics, University of Oslo, Oslo, Norway
- ²² Department of Physics and Technology, University of Bergen, Bergen, Norway
- ²³ Dipartimento di Fisica dell'Università 'La Sapienza' and Sezione INFN, Rome, Italy
- ²⁴ Dipartimento di Fisica dell'Università and Sezione INFN, Cagliari, Italy
- ²⁵ Dipartimento di Fisica dell'Università and Sezione INFN, Trieste, Italy
- ²⁶ Dipartimento di Fisica dell'Università and Sezione INFN, Turin, Italy
- ²⁷ Dipartimento di Fisica e Astronomia dell'Università and Sezione INFN, Bologna, Italy
- ²⁸ Dipartimento di Fisica e Astronomia dell'Università and Sezione INFN, Catania, Italy
- ²⁹ Dipartimento di Fisica e Astronomia dell'Università and Sezione INFN, Padova, Italy
- ³⁰ Dipartimento di Fisica 'E.R. Caianiello' dell'Università and Gruppo Collegato INFN, Salerno, Italy
- ³¹ Dipartimento DISAT del Politecnico and Sezione INFN, Turin, Italy
- ³² Dipartimento di Scienze e Innovazione Tecnologica dell'Università del Piemonte Orientale and INFN Sezione di Torino, Alessandria, Italy
- ³³ Dipartimento Interateneo di Fisica 'M. Merlin' and Sezione INFN, Bari, Italy
- ³⁴ European Organization for Nuclear Research (CERN), Geneva, Switzerland
- ³⁵ Faculty of Electrical Engineering, Mechanical Engineering and Naval Architecture, University of Split, Split, Croatia
- ³⁶ Faculty of Engineering and Science, Western Norway University of Applied Sciences, Bergen, Norway
- ³⁷ Faculty of Nuclear Sciences and Physical Engineering, Czech Technical University in Prague, Prague, Czech Republic
- ³⁸ Faculty of Science, P.J. Šafárik University, Košice, Slovakia
- ³⁹ Frankfurt Institute for Advanced Studies, Johann Wolfgang Goethe-Universität Frankfurt, Frankfurt, Germany
- ⁴⁰ Gangneung-Wonju National University, Gangneung, Republic of Korea
- ⁴¹ Gauhati University, Department of Physics, Guwahati, India
- ⁴² Helmholtz-Institut für Strahlen- und Kernphysik, Rheinische Friedrich-Wilhelms-Universität Bonn, Bonn, Germany
- ⁴³ Helsinki Institute of Physics (HIP), Helsinki, Finland
- ⁴⁴ High Energy Physics Group, Universidad Autónoma de Puebla, Puebla, Mexico
- ⁴⁵ Hiroshima University, Hiroshima, Japan
- ⁴⁶ Hochschule Worms, Zentrum für Technologietransfer und Telekommunikation (ZTT), Worms, Germany
- ⁴⁷ Horia Hulubei National Institute of Physics and Nuclear Engineering, Bucharest, Romania
- ⁴⁸ Indian Institute of Technology Bombay (IIT), Mumbai, India
- ⁴⁹ Indian Institute of Technology Indore, Indore, India
- ⁵⁰ Indonesian Institute of Sciences, Jakarta, Indonesia
- ⁵¹ INFN, Laboratori Nazionali di Frascati, Frascati, Italy
- ⁵² INFN, Sezione di Bari, Bari, Italy
- ⁵³ INFN, Sezione di Bologna, Bologna, Italy
- ⁵⁴ INFN, Sezione di Cagliari, Cagliari, Italy
- ⁵⁵ INFN, Sezione di Catania, Catania, Italy
- ⁵⁶ INFN, Sezione di Padova, Padova, Italy
- ⁵⁷ INFN, Sezione di Roma, Rome, Italy
- ⁵⁸ INFN, Sezione di Torino, Turin, Italy

- ⁵⁹ INFN, Sezione di Trieste, Trieste, Italy
- ⁶⁰ Inha University, Incheon, Republic of Korea
- ⁶¹ Institut de Physique Nucléaire d’Orsay (IPNO), Institut National de Physique Nucléaire et de Physique des Particules (IN2P3/CNRS), Université de Paris-Sud, Université Paris-Saclay, Orsay, France
- ⁶² Institute for Nuclear Research, Academy of Sciences, Moscow, Russia
- ⁶³ Institute for Subatomic Physics, Utrecht University/Nikhef, Utrecht, Netherlands
- ⁶⁴ Institute for Theoretical and Experimental Physics, Moscow, Russia
- ⁶⁵ Institute of Experimental Physics, Slovak Academy of Sciences, Košice, Slovakia
- ⁶⁶ Institute of Physics, Homi Bhabha National Institute, Bhubaneswar, India
- ⁶⁷ Institute of Physics of the Czech Academy of Sciences, Prague, Czech Republic
- ⁶⁸ Institute of Space Science (ISS), Bucharest, Romania
- ⁶⁹ Institut für Kernphysik, Johann Wolfgang Goethe-Universität Frankfurt, Frankfurt, Germany
- ⁷⁰ Instituto de Ciencias Nucleares, Universidad Nacional Autónoma de México, Mexico City, Mexico
- ⁷¹ Instituto de Física, Universidade Federal do Rio Grande do Sul (UFRGS), Porto Alegre, Brazil
- ⁷² Instituto de Física, Universidad Nacional Autónoma de México, Mexico City, Mexico
- ⁷³ iThemba LABS, National Research Foundation, Somerset West, South Africa
- ⁷⁴ Johann-Wolfgang-Goethe Universität Frankfurt Institut für Informatik, Fachbereich Informatik und Mathematik, Frankfurt, Germany
- ⁷⁵ Joint Institute for Nuclear Research (JINR), Dubna, Russia
- ⁷⁶ Korea Institute of Science and Technology Information, Daejeon, Republic of Korea
- ⁷⁷ KTO Karatay University, Konya, Turkey
- ⁷⁸ Laboratoire de Physique Subatomique et de Cosmologie, Université Grenoble-Alpes, CNRS-IN2P3, Grenoble, France
- ⁷⁹ Lawrence Berkeley National Laboratory, Berkeley, California, United States
- ⁸⁰ Lund University Department of Physics, Division of Particle Physics, Lund, Sweden
- ⁸¹ Nagasaki Institute of Applied Science, Nagasaki, Japan
- ⁸² Nara Women’s University (NWU), Nara, Japan
- ⁸³ National and Kapodistrian University of Athens, School of Science, Department of Physics, Athens, Greece
- ⁸⁴ National Centre for Nuclear Research, Warsaw, Poland
- ⁸⁵ National Institute of Science Education and Research, Homi Bhabha National Institute, Jatni, India
- ⁸⁶ National Nuclear Research Center, Baku, Azerbaijan
- ⁸⁷ National Research Centre Kurchatov Institute, Moscow, Russia
- ⁸⁸ Niels Bohr Institute, University of Copenhagen, Copenhagen, Denmark
- ⁸⁹ Nikhef, National institute for subatomic physics, Amsterdam, Netherlands
- ⁹⁰ NRC Kurchatov Institute IHEP, Protvino, Russia
- ⁹¹ NRNU Moscow Engineering Physics Institute, Moscow, Russia
- ⁹² Nuclear Physics Group, STFC Daresbury Laboratory, Daresbury, United Kingdom
- ⁹³ Nuclear Physics Institute of the Czech Academy of Sciences, Řež u Prahy, Czech Republic
- ⁹⁴ Oak Ridge National Laboratory, Oak Ridge, Tennessee, United States
- ⁹⁵ Ohio State University, Columbus, Ohio, United States
- ⁹⁶ Petersburg Nuclear Physics Institute, Gatchina, Russia
- ⁹⁷ Physics department, Faculty of science, University of Zagreb, Zagreb, Croatia
- ⁹⁸ Physics Department, Panjab University, Chandigarh, India
- ⁹⁹ Physics Department, University of Jammu, Jammu, India
- ¹⁰⁰ Physics Department, University of Rajasthan, Jaipur, India
- ¹⁰¹ Physikalisches Institut, Eberhard-Karls-Universität Tübingen, Tübingen, Germany
- ¹⁰² Physikalisches Institut, Ruprecht-Karls-Universität Heidelberg, Heidelberg, Germany
- ¹⁰³ Physik Department, Technische Universität München, Munich, Germany
- ¹⁰⁴ Research Division and ExtreMe Matter Institute EMMI, GSI Helmholtzzentrum für Schwerionenforschung GmbH, Darmstadt, Germany
- ¹⁰⁵ Rudjer Bošković Institute, Zagreb, Croatia
- ¹⁰⁶ Russian Federal Nuclear Center (VNIIEF), Sarov, Russia
- ¹⁰⁷ Saha Institute of Nuclear Physics, Homi Bhabha National Institute, Kolkata, India
- ¹⁰⁸ School of Physics and Astronomy, University of Birmingham, Birmingham, United Kingdom
- ¹⁰⁹ Sección Física, Departamento de Ciencias, Pontificia Universidad Católica del Perú, Lima, Peru
- ¹¹⁰ Shanghai Institute of Applied Physics, Shanghai, China

- 111 St. Petersburg State University, St. Petersburg, Russia
- 112 Stefan Meyer Institut für Subatomare Physik (SMI), Vienna, Austria
- 113 SUBATECH, IMT Atlantique, Université de Nantes, CNRS-IN2P3, Nantes, France
- 114 Suranaree University of Technology, Nakhon Ratchasima, Thailand
- 115 Technical University of Košice, Košice, Slovakia
- 116 Technische Universität München, Excellence Cluster 'Universe', Munich, Germany
- 117 The Henryk Niewodniczanski Institute of Nuclear Physics, Polish Academy of Sciences, Cracow, Poland
- 118 The University of Texas at Austin, Austin, Texas, United States
- 119 Universidad Autónoma de Sinaloa, Culiacán, Mexico
- 120 Universidade de São Paulo (USP), São Paulo, Brazil
- 121 Universidade Estadual de Campinas (UNICAMP), Campinas, Brazil
- 122 Universidade Federal do ABC, Santo Andre, Brazil
- 123 University College of Southeast Norway, Tonsberg, Norway
- 124 University of Cape Town, Cape Town, South Africa
- 125 University of Houston, Houston, Texas, United States
- 126 University of Jyväskylä, Jyväskylä, Finland
- 127 University of Liverpool, Liverpool, United Kingdom
- 128 University of Tennessee, Knoxville, Tennessee, United States
- 129 University of the Witwatersrand, Johannesburg, South Africa
- 130 University of Tokyo, Tokyo, Japan
- 131 University of Tsukuba, Tsukuba, Japan
- 132 Université Clermont Auvergne, CNRS/IN2P3, LPC, Clermont-Ferrand, France
- 133 Université de Lyon, Université Lyon 1, CNRS/IN2P3, IPN-Lyon, Villeurbanne, Lyon, France
- 134 Université de Strasbourg, CNRS, IPHC UMR 7178, F-67000 Strasbourg, France, Strasbourg, France
- 135 Université Paris-Saclay Centre d'Études de Saclay (CEA), IRFU, Department de Physique Nucléaire (DPhN), Saclay, France
- 136 Università degli Studi di Foggia, Foggia, Italy
- 137 Università degli Studi di Pavia and Sezione INFN, Pavia, Italy
- 138 Università di Brescia and Sezione INFN, Brescia, Italy
- 139 Variable Energy Cyclotron Centre, Homi Bhabha National Institute, Kolkata, India
- 140 Warsaw University of Technology, Warsaw, Poland
- 141 Wayne State University, Detroit, Michigan, United States
- 142 Westfälische Wilhelms-Universität Münster, Institut für Kernphysik, Münster, Germany
- 143 Wigner Research Centre for Physics, Hungarian Academy of Sciences, Budapest, Hungary
- 144 Yale University, New Haven, Connecticut, United States
- 145 Yonsei University, Seoul, Republic of Korea